V-shaped semisubmersible offshore wind turbine: An alternative concept for offshore wind technology

Karimirad, M., & Michailides, C. (2015). V-shaped semisubmersible offshore wind turbine: An alternative concept for offshore wind technology. *Renewable Energy*, *83*, 126-143. https://doi.org/10.1016/j.renene.2015.04.033

Published in:
Renewable Energy

Document Version:
Peer reviewed version

V-shaped semisubmersible offshore wind turbine: an alternative concept for offshore wind technology

Madjid Karimirad[a] and Constantine Michailides[b]

[a] *Norwegian Marine Technology Research Institute (MARINTEK), Marine Technology Centre, Otto Nielsens veg 10, NO-7052 Trondheim, Norway (Postal address: POB 4125 Valentinlyst, NO-7450 Trondheim, Norway), Email address: Madjid.Karimirad@marintek.sintef.no*

[b] *Centre for Ships and Ocean Structures (CeSOS), Department of Marine Technology, Norwegian University of Science and Technology (NTNU), Otto Nielsens vei 10, NO-7491, Trondheim, Norway; constantine.michailides@ntnu.no*

Abstract

The design aspects of a 5-MW V-shaped semisubmersible floating wind turbine considering the floater main dimensions and configurations are presented in this paper. Initially, the effect of different geometry parameters that correspond to different design cases have been investigated on the hydrostatic stability of the semisubmersible support platform through the comparison of righting arm and righting moments. Afterwards, the dynamic behavior and performance of the V-shaped semisubmersible wind turbine are presented for one of the examined design cases. Aero-hydro-servo-elastic numerical modeling has been applied for achieving coupled integrated time-domain analysis in order to investigate the dynamics of the V-shaped semisubmersible offshore wind turbine. The water depth is selected to be 100 m in order to study the feasibility of such concept in moderate water depth. The wave-induced as well as wave-wind-induced motions, tension of mooring lines and functionality of wind turbine are presented and discussed for selected environmental conditions. In general, the results show that the presented in the present paper V-shaped semisubmersible offshore wind turbine is a promising concept which can enhance the offshore wind industry.

Keywords: Floating wind turbine; V-shaped semisubmersible platform; Wave-wind-induced; Stochastic dynamics; Offshore wind technology.

1. Introduction

Offshore wind energy is widely recognized as a useful renewable energy capable to satisfy the increasing energy need and to increase globally the security of energy supplies. Compared to the other renewable energy resources that exist in the oceans such as waves and tides, wind energy resource exploitation and its related technology is considered as matured and rather well established mainly for fixed-bottom concepts and shallow water depths where several offshore wind turbines have been put into operation [1,2,3]. For every possible site for installation of offshore wind turbines and depending to wave and wind characteristics, seabed properties and social conditions, the usage of floating wind turbines at some water depth [4,5,6] is indicated as the most appropriate mainly due to cost related issues. The development of offshore wind turbines in deep waters requires further investigation. The issues related to design configuration of the support structure, installation, grid connection, operation and maintenance have significant effects on the cost of produced electricity. Hence, the feasibility of different floating concepts needs to be addressed and innovative support structures that may help maturing the offshore wind technology should be introduced and analyzed. Functionality, performance, dynamics, safety, cost and power-production of a specific design are the main parameters that define the feasibility and probability of success of a concept in industry (Karimirad [7]).

Compared to conventional fixed-bottom offshore wind turbines, floating offshore wind turbines require high fidelity aero-hydro-servo-elastic coupled numerical analysis tools for their integrated analysis and incorporate features as follow:

- they introduce very low frequency modes that can affect the aerodynamic damping and stability of the system,
- for the case of semisubmersible and spar buoy support structures, they have translational and rotational motions that can be coupled with the motions of the rotor-nacelle assembly,
- they anchored to the seabed with a mooring system which must be included in the overall analysis,
- they do not need to have a slender/cylindrical support structure; hence, the hydrodynamic radiation and diffraction can become important.

Different floating concepts (Figure 1) considering the stability method, overall submerged shape, dimensions, water surface area and mooring system can be imagined [8,9,10,11] such as spar-buoys [12,13,14,15], semisubmersible [16,17,18], barges [19] and tension leg platform [20,21,22].

[Figure 1]

The semisubmersible concept relies on large water plane area as well as on a fairly deep draft and ballasting to maintain stability. A basic advantage of the use of semisubmersible platform is that it can be fabricated onshore in controlled settings where quality is more easily assured and afterwards towed to its site, eliminating the need for expensive construction barges and marine cranes. Furthermore, concrete, steel or hybrid semisubmersible platform can be utilized.

Common offshore semisubmersible wind turbine designs consist of cylinders that are connected each other with braces [23,24] (e.g. a three-column semisubmersible in Figure 1). A disadvantage of the braces of the semisubmersible platform is that they are prone to fatigue [25]. Usually the braces are slender structural elements that connect the columns of the semisubmersible. The extensive hydro-aerodynamic loads on the columns will be transferred to these members. In short-crested sea conditions, the wave loads that are applied on each column have a specific phase; this phase results to cyclic loading at the root of the braces. The welded joints are exposed to stress concentration which results in fatigue damage in long term perspective. Furthermore, the axial forces (tension-compression) combined with periodic bending moments will result in accumulated damage. Due to the large difference between the diameter of the brace and columns punching may occur which should be checked as well.

Braceless semisubmersible platforms are widely and successfully deployed in offshore oil and gas industry. The same idea is used in order to introduce braceless semisubmersible offshore wind turbines [26,27,28,29,30]. These structures do not have braces and hence they are less prone to fatigue at the welded joints (Figure 2).

In the present paper design aspects of a 5-MW V-shaped semisubmersible offshore wind turbine considering the floater main dimensions and configurations are presented. Initially, the effect of different shape-parameters has been investigated on the hydrostatic stability of the semisubmersible support platform. Righting arm and righting moments are compared for the case of different examined design cases. For one selected design case wave-induced as well as wave-wind-induced motions, tension of mooring lines and functionality of wind turbine are presented and discussed for selected environmental conditions. The tool Simo-Riflex-Aerodyn has been used for the aero-hydro-servo-elastic dynamic analysis of the V-shaped semisubmersible offshore wind turbine. In general, the results show that the presented in the present paper V-shaped semisubmersible offshore wind turbine is a promising concept which can enhance the offshore wind industry.

[Figure 2]

2. Characteristics of the V-shaped semisubmersible platform and of the wind turbine

The V-shaped semisubmersible offshore wind turbine in the present paper consists of: (a) a semisubmersible floating platform with three columns (one central column and two side columns) and two pontoons connecting the side columns to the central column making a V-shape, (b) a 5 MW wind turbine placed top of the central column of the semisubmersible platform and (c) three catenary mooring lines positioned at the three columns of the semisubmersible. The 5 MW NREL wind turbine is located at the top of the column that is supported by both pontoons (Figure 3). Right handed coordinate system with Z-axis upward from mean sea level (MSL) is used. The wind and wave are propagating in positive X-direction. This means that in the head sea (zero for wave), the waves coming from left to right. Upwind turbine is put over the floater and the rotor blades have negative X-value position. With regard to geometry characteristics of the V-shaped semisubmersible platform, the three columns of the semisubmersible have the shape of cylinder; while the two fully submerged pontoons that are connect the three columns have rectangular shape. The two side columns have 20 m freeboard while the central one has 10 m freeboard. The draft of the semisubmersible platform is equal to 28 m. All the structural parts that compose the semisubmersible platform have thickness equal to 3 cm and have material properties that correspond to the properties of steel. It must be noted that the selection of the wall thickness to be equal to 3 cm is reasonable but a detailed engineering design is required in order to check if this thickness is sufficient or too large.

The NREL 5 MW wind turbine that has been applied is based on Jonkman et al. [31]. It should be stressed that the tower of the wind turbine is modified for floating wind turbine application according to Jonkman [32]. The main properties of the tower and wind turbine are listed in Table 1 and Table 2.

[Table 1]

[Table 2]

[Figure 3]

3. Hydrostatic stability of the semisubmersible platform

One of the main design aspects of marine structures is static stability. For floating structures, the hydrostatic stability which is related to static equilibrium of buoyancy and gravity forces is very important. There are rules and regulations available for offshore and ship structures addressing stability requirements under intact and damaged conditions [33,34]; meanwhile in [35] exists recommendations for stability analysis of floating wind turbines. However, since the offshore wind turbines are unmanned, there is a question regarding the "required" safety level (or safety target).

For a catenary moored semisubmersible platform, the effects of pre-tension and weight of mooring system are negligible compared to the total weight of the structure. The longitudinal metacentric height, GM_L, is tightly linked to tilt angle (which appears as pitch motion in dynamic context). Similarly, for heel angle (roll motions) the transversal metacentric height, GM_T, is important. In general, the transversal metacentric height of ship-shaped structures is much smaller than the longitudinal metacentric height. However, for symmetric offshore structures, transversal and longitudinal metacentric heights are more or less the same. It must be noted that the metacentric height is the distance between the center of gravity (CoG) and the metacenter of the semisubmersible platform.

Both the metacentric heights, GM_L and GM_T, have two contributing parts related to surface area effects and gravitational-buoyancy. For semisubmersible platforms, the main positive contributor is the surface area. Semisubmersible platforms use the advantageous of spreading the area which significantly helps to increase the area moment of inertia. As it is clear in Figure 3, the V-shaped semisubmersible structure is symmetric only in X axis. Hence, the metacentric heights in transversal and longitudinal directions can be different. The performance of the floating wind turbine depends upon different environmental conditions that include short-crested sea states, misalignment between wave and wind and different wave headings. As a result both the metacentric heights are important. Moreover, for this kind of structure the metacentric height is tightly linked to hydrostatic restoring moments as well as dynamic performance of the system.

In the following sub-sections, sensitivity studies considering the effect of angle between pontoons as well as the effect of pontoon/column dimensions on the stability of the V-shaped semisubmersible floating wind turbine are presented and discussed. The stability analysis has been performed with the use of the software HydroD [36]. For the calculation of the relation between the overturning moment and heeling angle, the effects of the mooring lines are included in the stability analysis.

3.1 Effect of angle between pontoons on the hydrostatic stability of the V-shaped floating wind turbine

In order to examine the effect of the angle between pontoons on the stability of the V-shaped semisubmersible floating wind turbine, the righting arm (GZ) and righting moment curves as a function of the heeling angles of four different examined cases are compared. Four different designs namely V55, V60, V65 and V75 denoting θ=55 deg, θ=60 deg, θ=65 deg and θ=75 deg, respectively, are studied. It must be noted that θ is the angle between pontoons (Figure 3). In Table 3, characteristics of the four different examined cases are listed related to the geometry of the semisubmersible as well as to the longitudinal, GM_L, and transversal, GM_T, metacentric heights as calculated from the stability analysis. It must be noted that with CoB the centre of buoyancy is symbolized. For all the examined cases the draft is equal to 28 m, the distance between the centreline of the columns is 60 m, the diameter of the columns is 7 m and the pontoon has a rectangular cross section with dimension 7x4 m. As it can be seen in Table 3, the gradually increase of the θ results to the gradually decrease of the GM_L and to the gradually increase of the GM_T. For θ=60 deg GM_L is equal with GM_T, GM_L=GM_T=4.3 m. In Figure 4 and Figure 5, the righting arm and righting moment curves, respectively, as calculated from the stability analysis are presented for the four examined cases, V55, V60, V65 and V75, for both transversal (around X axis) and longitudinal (around Y axis) direction.

As it is clear in Figure 4, all the designs will not be capsized at heeling angle less than 50 degrees. The maximum of the righting arm is changing depending to the different design and to the directionality of the applied heeling moment. Additionally, the righting moments are compared with a constant threshold moment value, T_{thres} (Figure 5). It is noted that the T_{thres} value has no connection and is not used in the stability analysis which performed with the use of the HydroD software. The T_{thres} moment value is defined by multiplying the maximum expected thrust force and the distance between top of tower and fairlead positions, T_{thres}=750x(90+18)=81,000 kNm. It must be noted that the maximum thrust occurs in operational conditions at rated-wind speed (11.4 m/sec). The fairleads are located 18 m below the MSL and the nacelle-hub height is 90 m above the MSL. The required righting moment for such heeling moment appears at heeling angle of 16 deg for V55 and V60, of 18 deg for V65 and of 23 deg for V75. As it is clear in Figure 4 and Figure 5, the GZ curves and righting moments in translational and longitudinal directions are very similar for V60 in particular for small heeling angles, α. This can be explained since the metacentric heights, GM_L and GM_T, and consequently the righting moments in translational and longitudinal directions are almost equal for V60. It must be noted that for small heeling angles, α, $GZ=GM_L x\sin\alpha$ and $GZ=GM_T x\sin\alpha$, which is consistent with the results that are presented in Figure 4.

[Table 3]

[Figure 4]

[Figure 5]

3.2 Effect of pontoons/columns dimensions on the hydrostatic stability of the V-shaped floating wind turbine

In the previous sub-section, the effect of the angle between pontoons is explained. Here, the pontoon and column dimensions are modified in order to study the effects of this modification on the hydrostatic stability of the V-shaped semisubmersible. The V60 (sub-section 3.1) is selected as the base configuration. The V60 design is compared with three alternative designs: (a) decreasing the length between columns (50 m) and increasing the pontoon section (9x5 mxm) and columns diameter (9 m), $V60_{al1}$, (b) increasing the length of pontoon (70 m), $V60_{al2}$, and (c) increasing the column diameter (9 m) and increasing the pontoon section (9x5 mxm), $V60_{al3}$. Characteristics of the three aforementioned alternative designs are listed in Table 4. For all the examined alternative cases the draft is kept equal to 28 m.

In Figure 6 and Figure 7 the righting arm and righting moment curves, respectively, are presented as a function of the heeling angle for V60, $V60_{al1}$, $V60_{al2}$ and $V60_{al3}$. Considering the results that are presented in Figure 6 and Figure 7, the $V60_{al3}$ design is selected for further investigation regarding the performance and dynamics of the system in the rest of the paper. This design, $V60_{al3}$, has just 6 degrees of heel under the defined threshold, T_{thres}. This means the rotor swept area is expected to subjected to 0.4% reduction for the rated wind speed loading in calm sea. But, due to wave and wind loads and dynamic responses, the tilt angle will increase which decrease the rotor swept area and consequently the power production of the system. If the tilt angle increase to double due to pitch motion and coupled dynamics, the power production will decrease by 1.5% (roughly). The dynamic behavior, functionality and power performance of the $V60_{al3}$ design will be discussed in the following sections of the present paper.

[Table 4]

[Figure 6]

[Figure 7]

4. Numerical modeling of the floating wind turbine

For the high fidelity modeling and analysis of the V-shaped floating wind turbine, the following codes are used, directly or indirectly as an input for the final hydro-aero-servo-elastic time domain analysis. In Table 5 the mass moment of inertia as well as the coordinates of the CoB and CoG of the $V60_{al3}$ is listed. All the inertias are given with respect to the MSL. It must be noted that in the present paper any possible kind of active water ballast system into the three columns of the semisubmersible platform is not considered and not included in the analysis. In Figure 8, examples of modeling are illustrated. The codes that are used are:

- Genie [37]: Modeling the geometry, mass/inertia properties and creating the panel model for hydrodynamic analysis,
- WAMIT [38]: Hydrodynamic analysis of the wet surface of the platform in frequency domain,
- SIMA [39]: Coupled mooring-floater dynamic analysis,
- Simo [40] –Riflex [41]: Integrated wave-induced simulations,
- Simo-Riflex-Aerodyn [42]: Hydro-aero-servo-elastic time domain analysis.

[Table 5]

[Figure 8]

4.1 Mooring lines configuration

Three mooring lines are used with one clump mass for each. The mooring line configuration has symmetry with respect to the XZ plane. The properties of the mooring lines are given in Table 6. In Table 6 the term equivalent axial stiffness is defined as the product of the modulus of elasticity of the material of the mooring lines with the area of the cross section of the mooring lines. Also, the equivalent axial stiffness is defined as the product of the modulus of elasticity of the material of the mooring lines, E, with the area, A, of the cross section of the mooring lines. The chosen specific values in Table 6 correspond to representative values for mooring lines that behaves as multi-strand wire rope. Mooring lines' stiffness consists of material and geometrical stiffness. The force-displacement properties of a catenary moored system are dependent on material properties, line geometry and mooring system configuration. The geometrical stiffness is the main contributor for catenary mooring systems in most cases. The geometrical stiffness of catenary mooring system is a function of mooring line length, clump mass, buoyancy elements, fairlead position and footprint of anchoring system. In the present paper, some initial analyses have been performed to select the mooring system geometry and mooring line properties. In such consideration the dynamics of the floating wind turbine as well as mooring tension responses have been considered to avoid over-loading and slack of mooring lines.

The fairlead and anchoring positions are listed in Table 7. The static configuration and effective tension of the used catenary mooring lines are presented in Figure 9 and Figure 10, respectively.

It is necessary to mention that the different designs that are presented in this study are not optimized with respect to the cost and the structural integrity of different parts of the V-shaped semisubmersible wind turbine. The dimensions and properties utilized in this study are selected in the basis to present rational designs. The aim of the present study is to investigate the feasibility of the V-shaped concept. Hence, optimization including detailed engineering design is out of the scopes of the present paper.

[Table 6]

[Table 7]

[Figure 9]

[Figure 10]

4.2 Natural frequencies and hydrodynamic characteristics

Added mass and restoring coefficients of the $V60_{al3}$ are listed in Table 8 and Table 9, respectively. The restoring coefficients C_{55} and C_{44} are calculated with respect to the coordinate system as presented in Figure 3. The area moment of inertia around X and Y axis are not the same in the defined coordinate system and as a result the corresponding restoring values are different. It must be noted that the numerical equations in Simo-Riflex-Aerodyn were set with respect to the defined coordinate system.

[Table 8]

[Table 9]

According to empirical formulas the roll and pitch natural frequencies can be estimated by (ignoring the coupling effects):

$$\omega_{roll} = \sqrt{(K_{44})/(I_{xx} + A_{44})} = \sqrt{(7.86\exp.+8)/(1.29\exp.+10 + 5.488\exp.+9)} = 0.20\text{rad/sec}$$

$$\omega_{pitch} = \sqrt{(K_{55})/(I_{yy} + A_{55})} = \sqrt{(3.07\exp.+9)/(2.18\exp.+10 + 1.022\exp.+10)} = 0.31\text{rad/sec}$$

Based on decay and dynamic analyses, the heave natural frequency is around 0.25 rad/sec. It must be noted that the aforementioned responses of the platform are coupled. However, it is possible to assume initially that the motions are uncoupled in order to investigate the natural frequencies of the system by empirical formulas (as estimated above for roll and pitch motions) that in most of the cases provide a good rough estimation of the natural frequencies of the system. However, the drift motion induced by wave and wind loads, nonlinear load actions and damping affect the natural frequencies. Moreover, the coupling between different modes alters the hydrostatic stiffness, which in taut system has a large influence (i.e. for tension leg platforms). The V-shaped semisubmersible is catenary moored and hence the platform motions are not linked through mooring lines which is the case for taut moored structures

[43]. As far as surge, sway and yaw motions there is no hydrostatic restoring and hence, natural frequencies of these modes tightly linked to mooring line stiffness. The force-displacement relation for mooring system is usually nonlinear, especially for floating wind turbines due to offset caused by mean wind loads and wave drift loads. This means natural frequency of these slowly-varying modes can be modified in different environmental conditions, load cases and turbine status.

5. Stochastic dynamics

5.1 Wave only load cases

5.1.1 Extreme sea state

An extreme wave condition with significant wave height, H_s, 14.4 m and wave spectral peak period, T_p, 13.3 sec is applied in order to investigate the mooring system performance as well as motions' characteristics. It must be noted that the chosen sea states are related with a specific offshore area in North Sea off the Norwegian coast [3]. The head-sea (wave heading of 0 degrees) and quarter-sea (wave heading of 45 degrees) are considered. Statistical quantities of one hour simulation of the mooring line tension and motions are listed in Table 10. In Figure 11 the motion response spectra of surge, sway, heave, roll, pitch and yaw for wave heading of 45 degrees are presented. The wave frequency and natural frequency responses are indicated for each mode of response. In general, the eigenfrequencies are well set out of first-order wave frequency excitation. The time series and spectra of effective tension of mooring lines are presented in Figure 12 and Figure 13, respectively. It must be noted that in the presented results the overall simulation time for each examined environmental condition is 4,100 sec; the first 500 sec have not been considered in order the effects from the turbine run-up not to be accounted. As the stochastic analysis in time domain present transient parts that should be avoided prior to statistical and spectral analysis, hence, the first 500 seconds of the time domain simulations are neglected. The statistical and spectral analyses are based on the time duration between 500 and 4,100 seconds (1 hour simulation). The statistical quantities that are presented in Table 10 are based to 1 hour simulation and they cannot be considered as extreme predicted values. In Table 10 the mean, standard deviation, minimum and maximum values of each 1 hour simulation are presented and symbolized with Mean, STD, Min and Max, respectively. These values are presented in order to compare the wave heading effect on the different motions. For the examined extreme sea states the maximum utilization, U, of the mooring lines is:

$$\sigma = T_e / A = 2,720\text{kN} / 0.01496\text{m}^2 = 181\text{MPa}$$

$$U = (\sigma \times R_S)/(\sigma_y / R_M) = (181 \times 1.3)/(350/1.15) = 0.77$$

where σ is stress, T_e is effective tension, A is area of the cross section of the mooring line, R_s is a safety load factor and R_M is a safety material factor. The minimum breaking load of mooring lines accounting for the material and load factors is 3,502 kN.

[Table 10]

[Figure 11]

[Figure 12]

[Figure 13]

As it is clear in Figure 11, the spectra of the motions of the semisubmersible platform under the action of waves consist of two parts: (a) the low frequency part, which is related to resonant responses of the platform and (b) the wave frequency part. Some motions are coupled and hence more than one peak is observed at low frequency part (both surge and pitch resonant peaks are presenting for surge spectrum). The resonant frequencies as appeared in dynamic responses are very close to the values that have been calculated by empirical formula (sub-section 4.2). The small differences in the natural frequencies are explained by the coupling effects between different motions, damping effects and involved nonlinearities.

In Figure 12, there is a large difference between tension responses of upstream and downstream mooring lines. This is observed since ML1 is the only mooring line acting downstream. Hence, the tension of ML1 obtains larger values than the tension of ML2 and ML3.

In Figure 13, the spectra of the tension responses are presented. As it is clear, the tension response consists of three parts. The low frequency part is related with slowly-varying motions such as surge, sway and yaw. In the wave frequency part, an obvious peak around 0.5 rad/sec exists and in the high frequency part, the elastic eigenfrequencies are presented. These eigenfrequencies are excited by harmonics of wave loads. The quadratic hydrodynamic damping effectively reduces the effect of these eigenfrequencies in the high frequency part [44].

5.1.2 Moderate sea state

The behavior of the V-shaped semisubmersible in moderate sea sate has been investigated. A sea state with significant wave height, H_s, 3 m and wave spectral peak period, T_p, 10 sec is applied in order to investigate the mooring system performance as well as motions' characteristics. Quarter-sea (wave heading of 45 degrees) is considered. In Figure 14 the motion response spectra of surge, sway, heave, roll, pitch and yaw motions for wave heading of 45 degrees are presented. It can be seen that the eigenfrequencies are well set out of first-order wave-frequency excitation. In Figure 15 time series of motions are presented. The time series of the motions correspond to the origin (0,0,0) of the global coordinate system that is used (Figure 3). The time series and spectra of effective tension of mooring lines are presented in Figure 16 and Figure 17, respectively.

As it is clear in Figure 14, the spectra of the motion responses consist of two parts. The low frequency part is related with the resonance of the motions while the higher frequency part is related with wave-induced motions. This is similar to what is observed for wave-induced responses of the platform under extreme sea state (sub-section 5.1.1). Compared to extreme sea state, the main difference is that the magnitude of the motions is extensively smaller in moderate sea state but with the same trend. As far as the tension responses of the mooring lines and compared to extreme sea state, same trend is observed for moderate sea state. The magnitude of the tension response is smaller for moderate sea state for all the mooring lines. Also, the dynamics of the tension responses is reduced, which is clear when comparing Figure 12 and 16.

In Figure 17, the spectra of the tension responses in moderate sea state are presented. The spectra of the tension responses are mainly dominated by slowly varying motions. The higher frequency parts, i.e. the wave frequency region does not appear for such moderate sea state while for extreme sea state the wave frequency part has appeared clearly (Figure 13) and dominates the tension responses.

[Figure 14]

[Figure 15]

[Figure 16]

[Figure 17]

5.2 Wave and wind load cases

5.2.1 Rated wind speed

The performance of the V-shaped wind turbine subjected to environmental condition corresponding to rated wind speed is investigated in the present sub-section. The mean wind speed of 11.4 m/sec with turbulence intensity of 0.15 is applied in order to create a turbulence box that is required for the coupled wave and wind induced analysis. Correlated with the rated wind speed of 11.4 m/sec, the significant wave height is 3 m and the peak period is 10 sec. In Figure 18 time series of motions for head sea wave direction and aligned wind direction are presented. The corresponding spectra of the motion responses are presented in Figure 19. The time series and spectra of effective tension of mooring lines are presented in Figure 20 and Figure 21, respectively. Compared to the wave only load cases (sub-section 5.1.1 and 5.1.2), it is clear that the responses that correspond to wave and wind load cases are increased due to additional wind excitation. Most of the responses are affected at natural frequencies due to concentrated energy of wind in low frequency part, as it was expected.

The surge motion time series (Figure 18) and the corresponding spectrum of surge motion (Figure 19) have very low frequency components. This is observed since the wind energy exists at low frequencies. In fact, the wind spectrum has an extensive energy with large return period in the order of 1,000 seconds and consequently the semisubmersible wind turbine is exposed to load actions with very low frequency components. As a result the slowly varying motions of the platform such as surge, sway and yaw are affected and response components with high return periods are observed. The wave-wind-induced motions presented in Figure 19 have the same frequency components as the wave-only responses presented in Figure 14. However, the magnitude of the slowly varying motions are affected by the wind actions and larger resonant responses are observed for the case of wave-wind-induced load cases. In some cases, the wind loads are completely governing the motion of the platform; the response of the yaw motion is governed by wind action (Figure 19). As it clear in Figure 21, the tension responses in coupled wave-wind-induced analyses are mainly governed by wind actions. This is linked to yaw resonant responses at 0.08 rad/sec which is excited by wind energy at low frequencies.

The wind speed, rotational speed of rotor, blade-pitch-angle, generated power and nacelle surge acceleration time series and spectra are presented in Figure 22 and Figure 23, respectively. In Figure 22, it is clear that there is no blade-pitch control for specific time durations. This happens as the relative wind speed recognized by the blades is less than rated wind speed for specific time durations. Hence, the wind turbine is working below rated wind speed for those durations of time. It must be noted that the maximum acceleration at nacelle (top of tower) is less than 0.2g (g is the gravitational acceleration). In general, the wind turbine manufactures suggest that the maximum acceleration should be always less than 0.5g in order to avoid damage to drivetrain components [45]

When the wind turbine is in operation for below rated wind speed condition, the control of wind turbine is limited to torque control which shows itself in rotational speed of the rotor. The target of the controller in this region is to take off the maximum power from the aerodynamic kinetic energy. This means the entire energy of wind containing all frequency components will affect the floating wind turbine. As it is discussed before, wind has great energy at low frequencies which can excite low frequency responses of the platform. Figure 23 shows the spectra of the turbine functionality data such as generated power. Most of responses of the turbine are governed by wind actions rather wave and this is clear as the responses have low frequency components close to zero rad/sec.

[Figure 18]

[Figure 19]

[Figure 20]

[Figure 21]

[Figure 22]

[Figure 23]

5.2.2 Over rated wind speed

The performance of the V-shaped wind turbine subjected to environmental condition corresponding to over rated wind speed is investigated below. The mean wind speed of 18 m/sec with turbulence intensity of 0.15 is applied. The significant wave height of 4.2 m and peak period of 10.5 sec are correlated with rated wind speed of 18 m/sec. In Figure 24 time series of motions for head sea wave direction and aligned wind are presented; the corresponding spectra of the motion responses are presented in Figure 25. The time series and spectra of effective tension of mooring lines ML1, ML2 and ML3 are presented in Figure 26 and Figure 27, respectively. The wind speed, rotational speed of rotor, blade-pitch-angle, generated power and nacelle surge acceleration time series and spectra are presented in Figure 28 and Figure 29, respectively.

In general the dynamic behavior of the semisubmersible wind turbine for over rated wind speed has same trends with the behavior for rated wind speed. The reason is that in rated wind speed the maximum aerodynamic loads that are occurred can govern the responses. Compared to rated wind speed, the tension response is smaller for over rated wind speed.

As it is mentioned, there are some differences between responses for over rated wind speed and rated wind speed. The resonant responses of the floating wind turbine for rated wind speed is slightly higher, which is related to the control effects of blade pitching for over rated wind speed load case that has as a result the reduction of the amplitude of the motions by aerodynamic damping. The peaks in the spectra of the responses are observed for similar values compared to what has been observed for rated wind speed. These peaks are related with the resonant responses of the floating wind turbine plus the wave frequency part. The wave frequency part in heave motion have a clear appearance (Figure 25); this is due to the fact that the wind forces have small components in heave direction while the first order wave loads are governing the heave motion, which is clear in wave-only responses (Figure 11 and 14).

Comparing the tension responses of the rated wind speed and over rated wind speed load cases, it is clear that the magnitude of responses has the same order of magnitude (Figure 20 and 21 against Figure 25 and 26). However, if the wave-only responses (Figure 16 and 17) are compared with the wave-wind-induced responses, it is clear that although the mean of tension responses are more or less the same but the tension response dynamics is higher for coupled wave-wind load cases due to excitation of low frequency responses. The low frequency responses can be excited by wind energy which is linked to turbulent features of wind.

The responses presented in Figure 28 and Figure 29 show that for the V-shaped semisubmersible wind turbine, the turbine functionality is not significantly affected by wave loads. As it is clear, the responses have very low frequency components excited by wind actions. The power production fluctuation has return period larger than 50 second. In a farm configuration, the output power from substation can be smoothed by summing up produced power from different turbines.

The electrical torque (Figure 30) is constant for over-rated wind speed case. The target of controller for over rated wind speed is set to constant torque to limit the aerodynamic loads and help structural integrity of the system. Also, in Figure 31, the rotor aerodynamic power spectrum is presented. The rotor harmonics are appearing in the aerodynamic power spectrum. In most of load cases, these harmonics are filtered by generator actions and hence the generated power will not have such high frequency components.

Comparing aerodynamic power (Figure 31) and electric power (Figure 29), it is obvious that the controller action is actively filtering the high frequency components while it cannot filter the low frequency part. This is due to the fact that the servo and controller have action frequency around 0.2 rad/sec, which means the phenomena with lower frequencies will not be affected by servo actions i.e. feathering the blades.

[Figure 24]

[Figure 25]

[Figure 26]

[Figure 27]

[Figure 28]

[Figure 29]

[Figure 30]

[Figure 31]

6. Conclusions

In the present paper, design aspects of a V-shaped braceless semisubmersible offshore wind turbine focusing on the static and dynamic response analysis and performance of the structure under actions of wave and wind loads are highlighted. The stability of the system for seven different examined design cases is studied. The hydrostatic stability characteristic of such system is highly linked to the dynamic performance of the system as the semisubmersible platforms are hydrostatically stabilized without the action of mooring lines. Hence, metacentric height of the system can represent the restoring moments in dynamics. This makes it easy to investigate the dimensioning of the floating part by setting heeling moment thresholds. The tilt/heel angle can affect the swept area of the turbine and consequently the produced electricity. Hence, large metacentric height is needed to restore the structure under wind and wave heeling moments. On the other hand, large metacentric height means high stiffness which may result in high natural period of the system hitting wave energy zone. By considering these points and similar aspects explained in the paper, the best possible solution among analyzed designs is finally selected for fully coupled dynamic analysis and further investigations.

Wave only load cases for extreme and moderate environmental conditions are studied in order to examine the behavior of the concept subjected to wave actions and also to examine the possible platform mooring lines coupling (especially the possible effects on the tension responses). The wave only extreme conditions are studied for two different wave propagating directions; this allows to examine the transversal motions (sway, roll and yaw) more easily. The yaw wave moments are huge for this kind of structure for oblique waves; however, the yaw inertia of the system is high enough to control the yaw motions, effectively. Tension responses are fairly reasonable even for 100 m water depth. In the examined designs, a catenary mooring system has been desired and matched by setting proper combination of line properties, clump mass and more specifically the line length between fairleads and anchoring points. The moderate sea state corresponds to rated wind speed load case. Compared to moderate sea state, the calculated responses for extreme conditions are more wave-frequency dominant while resonant responses are dominating the responses for moderate sea states. The reason is that the resonant frequencies of the structure are out of the wave zone, hence the magnitude of them will not be significantly changed by changing the wave height and they are controlled by the hydrodynamic damping. However, when the wave height increase in extreme load case the wave-frequency part increases and dominates the total dynamic response. The same trend is clear in tension responses.

As far as wave-wind load cases, both rated wind speed and over-rated wind speed load cases are analyzed in the present study. The rated wind speed is connected with maximum thrust force. Comparing the wave-only load case and wave-wind load case it is clear that in general, responses are increased due to additional wind excitation. Most of the responses are affected at natural frequencies as expected due to concentrated energy of wind in low frequency part. The performance of the wind turbine is highlighted by showing the electrical power production, rotational speed of rotor, blade-pitch-angle and nacelle acceleration. The spectral analysis shows that the performance of the wind turbine is highly affected by wind energy concentration at low-frequencies. It is not possible to enhance the turbine performance much with respect to the slowly-varying motion components as the resonant responses are anyway in the wind energy zone and will be excited. Note that the responses of the structure under action of wave and wind are inherently resulted of both aero-hydro excitation and damping actions.

For over-rated wind speed case, the electrical produced power has much less fluctuations around the mean value. The motion responses as well as tension of mooring lines are in good order. The trend of responses is more or less similar to rated-wind speed case. The electric torque is perfectly constant as it is set by target of the controller in this case. The aerodynamic power of the rotor has some high-frequency components related to rotor harmonics which are filtered by generator actions. Hence, the generated power has slowly-varying frequency components coming from rigid body resonant response induced by wind loads. The period of such components is higher than 20 seconds. Usually, combining generated power from array of wind turbines can help smoothing and filtering the remained fluctuations from slowly-varying wind-induced load and load-effects.

In general, the studies carried out in this paper highlight the feasibility of application of a braceless V-shaped semisubmersible wind turbine as an innovative solution for offshore wind technology. However, the presented results in the present paper give an idea (indicator) about the magnitude that the structural responses have for specific environmental conditions and more studies must be performed in future in order to investigate the proposed concept in more detail as well as to predict the extreme responses based on an appropriate long-term analysis.

Acknowledgements

The authors would like to thank the reviewers of this paper for their valuable comments and contribution to the improvement of the manuscript.

References

[1] Breton SF, Moe G. Status, plans and technologies for offshore wind turbines in Europe and North America. Renewable Energy 2009;34(3):646-654.

[2] Shi W, Park H, Han J, Na S, Kim C. A study on the effect of different modeling parameters on the dynamic response of a jacket-type offshore wind turbine in the Korean Southwest Sea. Renewable Energy 2013;58:50-59.

[3] Shi W, Han J, Kim C, Lee D, Shin H, Park H. Feasibility study of offshore wind turbine substructures for southwest offshore wind farm project in Korea. Renewable Energy 2015;74:406-413.

[4] Musial W, Butterfield S, Ram B. Energy from offshore wind. Offshore Technology Conference Houston, Texas, USA, 2006;1888-1898.

[5] Myhr A, Bjerkseter C, Ågotnes A, Nygaard TA. Levelised cost of energy for offshore floating wind turbines in a life cycle perspective. Renewable Energy 2014;66:714-728.

[6] Sun X, Huang D, Wu G. The current state of offshore wind energy technology development. Energy 2012;41:298-312.

[7] Karimirad M. Offshore Energy Structures. Switzerland: Springer; 2014.

[8] Karimirad M. Stochastic Dynamic Response Analysis of Spar-Type Wind Turbines with Catenary or Taut Mooring Systems. Thesis in partial fulfillment of the Doctor of Philoshophy degree, submitted to and defended in the Department of Marine Technology, Norwegian University of Science and Technology, 2012.

[9] Butterfield S, Musial W, Jonkman J, Sclavounos P. Engineering challenges for floating offshore wind turbines. Copenhagen Offshore Wind Conference, Copenhagen, Denmark, 2005.

[10] Hall M, Buckham B, Crawford C. Hydrodynamics-based floating wind turbine support platform optimization: A basis function approach. Renewable Energy 2014;66:559-569.

[11] Bagbanci H, Karmakar D, Guedes Soares C. Review of offshore floating wind turbine concepts, Maritime Engineering and Technology. C. Guedes Soares et al. (Eds.), Taylor & Francis Group, London, 2012: 553–562.

[12] Karimirad M, Moan T. Feasibility of the Application of a Spar-type Wind Turbine at a Moderate Water Depth. Energy Procedia 2012;24:340-350.

[13] Karimirad M, Moan T. (2012). Stochastic dynamic response analysis of a tension leg spar-type offshore wind turbine. Wind Energy 2012;16(6):953–973.

[14] Sethuraman L, Venugopal V. Hydrodynamic response of a stepped-spar floating wind turbine: Numerical modelling and tank testing. Renewable Energy 2013;52:160-174.

[15] Nava V, Guedes Soares C, Arena F.On the assessment of extreme forces on a floating spar wind turbine, Developments in Maritime Transportation and Exploitation of Sea Resources, C. Guedes Soares and López Peña (Eds.), Taylor & Francis Group, London 2012:553–562.

[16] Robertson A, Jonkman J, Masciola M, Song H, Goupee A, Coulling A, Luan C. Definition of the Semisubmersible Floating System for Phase II of OC4. NREL/TP-5000-60601, National Renewable Energy Laboratory, Golden, CO, U.S.A, 2014.

[17] Bagbanci, H., Karmakar, D., and Guedes Soares, C. Comparison of spar-type and semi-submersible type floaters concepts of offshore wind turbines using long term analysis, 32nd Int. Conf. Ocean, Offshore and Arctic Engineering, 2013, OMAE2013-11204.

[18] Lefebvre S, Collu M. Preliminary design of a floating support structure for a 5MW offshore wind turbine. Ocean Engineering 2012;40:15-26.

[19] Philippe M, Babarit A, Ferrant P. Modes of response of an offshore wind turbine with directional wind and waves. Renewable Energy 2013;49:151-155.

[20] Jonkman JM, Matha D. Dynamics of offshore floating wind turbines-analysis of three concepts. Wind Energy 2011;14(4):557–569.

[21] Bachynski EE, Moan T. Design considerations for tension leg platform wind turbines. Marine Structures 2012;29(1):89-114.

[22] Adama F, Myland T, Schuldt B, Großmann J, Dahlhaus F. Evaluation of internal force superposition on a TLP for wind turbines. Renewable Energy 2014;71:271-275.

[23] Roddier D, Cermelli C, Aubault A, Weinstein A. WindFloat: A floating foundation for offshore wind turbines. Journal of Renewable and Sustainable Energy 2010;2(3): 033104-1-033104-34.

[24] Roddier D, Cermelli C, Weinstein A. WindFloat: A Floating Foundation for Offshore Wind Turbines Part I: Design Basis and Qualification Process. 28th International Conference on Offshore Mechanics and Arctic Engineering 2009, OMAE2009-79229.

[25] Kvittem MI, Moan T, Gao Z, Luan C. Short-Term Fatigue Analysis of Semi-Submersible Wind Turbine Tower. 30th International Conference on Ocean, Offshore and Arctic Engineering, Rotterdam, The Netherlands, 2011, OMAE2011-50092.

[26] Olav Olsen AS, (Online). Available at: http://www.olavolsen.no/node/82 [Accessed 14 February 2015].

[27] Fukushima FORWARD, (Online). Fukushima Floating Offshore Wind Farm Demonstration Project. Japan: Fukushima Offshore Wind Consortium. Available at: http://www.fukushima-forward.jp/english/pdf/pamphlet3.pdf [Accessed 14 February 2015].

[28] Michailides C, Luan C, Gao Z, Moan T. WindFloat: Effect of Flap Type Wave Energy Converters on the Response of a Semi-submersible Wind Turbine in Operational Conditions. 33rd International Conference on Offshore Mechanics and Arctic Engineering 2014, OMAE2014-24065.

[29] Michailides C, Gao Z, Moan T. Response Analysis of the Combined Wind/Wave Energy Concept SFC in Harsh Environmental Conditions. 1st International Conference on Renewable Energies Offshore 2014, RENEW2014.

[30] Huijs F, Bruijn R, Savenije F. Concept design verification of a semi-submersible floating wind turbine using coupled simulations. Energy Procedia 2014;53:2-12.

[31] Jonkman J, Butterfield S, Musial W, Scott G. Definition of a 5-MW Reference Wind Turbine for Offshore System Development. NREL/TP-500-38060, National Renewable Energy Laboratory, Golden, CO, U.S.A, 2009.

[32] Jonkman, J. Definition of the Floating System for Phase IV of OC3. NREL/TP-500-47535, National Renewable Energy Laboratory, Golden, CO, USA 2010.

[33] IMO 2008. International Code on instact Stability (2008 IS CODE).

[34] IMO 2009. International Convention for the Safety of Life at Sea (SOLAS 2009).

[35] DNV 2013. DNV-OS-J103 Design of Floating Wind Turbine Structures.

[36] DNV (Det Norske Veritas) software SESAM, Norway, HydroD.

[37] DNV (Det Norske Veritas) software SESAM, Norway, Genie.

[38] WAMIT. WAMIT User Manual – program version 6.4, 2009.

[39] SIMA. SIMA User's Manual, MARINTEK 2014.

[40] SIMO. SIMO User's Manual, MARINTEK 2011a.

[41] RIFLEX. RIFLEX User's Manual, MARINTEK 2011b.

[42] Ormberg H, Bachynski EE. Global Analysis of Floating Wind Turbines: Code Development, Model Sensitivity and Benchmark Study. In: Proc of the 22nd International Off and Pol Eng Conf, June 17-22, Rhodes, Greece, 2012.

[43] Karimirad M, Meissonnier Q, Gao Z, Moan T. Hydro-elastic Code-to-Code Comparison for a Tension Leg Spar Type Floating Wind Turbine. Marine Structures 2011;24(4):412-435.

[44] Karimirad M. Modeling Aspects of a Floating Wind Turbine for Coupled Wave-wind-induced Dynamic Analyses. Renewable Energy 2013;53:299-305.

[45] Karimirad M, Moan T. A simplified method for coupled analysis of floating offshore wind turbines. Marine Structures 2012;27:45-63.

Table Captions

Table 1: Characteristics of the tower of the wind turbine [32]

Table 2: Characteristics of the wind turbine [31,32]

Table 3: Characteristics of different designs of V-shaped semisubmersible, V55, V60, V65 and V75, considering the modification of the angle between pontoons, θ.

Table 4: Characteristics of alternative designs of V-shaped semisubmersible considering increased pontoon and columns dimensions

Table 5: CoB, CoG and mass moment of inertia of the $V60_{al3}$

Table 6: Mooring line characteristics

Table 7: Coordinates of fairlead and anchoring points of the mooring lines ML1, ML2 and ML3

Table 8: Added mass coefficients calculated in WAMIT (at infinite frequency)

Table 9: Hydrostatic restoring coefficients calculated in WAMIT

Table 10: Statistical characteristics of motion and tension responses for wave only extreme environmental conditions

Figure Captions

Figure 1: Different floating concepts: semisubmersible, spar buoy and tension leg platform

Figure 2: Braceless semisubmersible offshore wind turbine (Fukushima FORWARD [12])

Figure 3: Schematic layout of the V-shaped semisubmersible offshore wind turbine

Figure 4: Transversal (around X-axis) and longitudinal (around Y-axis) GZ (righting arms) curves of V55, V60, V65 and V75 V-shaped semisubmersible offshore wind turbine

Figure 5: Transversal (around X-axis) and longitudinal (around Y-axis) righting moment curves of the V55, V60, V65 and V75 V-shaped semisubmersible offshore wind turbine

Figure 6: Transversal (around X-axis) and longitudinal (around Y-axis) GZ (righting arms) curves of $V60_{al1}$, $V60_{al2}$, $V60_{al3}$, and V60 V-shaped semisubmersible offshore wind turbine

Figure 7: Transversal (around X-axis) and longitudinal (around Y-axis) righting moment curves of the $V60_{al1}$, $V60_{al2}$, $V60_{al3}$, and V60 V-shaped semisubmersible offshore wind turbine

Figure 8: Modeling of the V-shaped semisubmersible: a) mooring lines and platform in SIMA, b) panel mesh for half-geometry in WAMIT (15,640 elements for entire platform) and c) V-shaped floating wind turbine in Genie

Figure 9: Static equilibrium configuration of catenary mooring lines

Figure 10: Axial effective tension in mooring lines in static equilibrium configuration, the clump mass effect is clear at X=82 m to increase the tension at upper part of the line from 930 kN to 1057 kN

Figure 11: Motion response spectra of surge, sway, heave, roll, pitch and yaw motions for wave heading of 45 degrees.

Figure 12: Time series of tension of mooring lines in extreme conditions for wave heading of 45 degrees

Figure 13: Spectra of tension of mooring lines in extreme sea state for wave heading of 45 degrees

Figure 14: Motion response spectra of surge, sway, heave, roll, pitch and yaw motions for a moderate sea state with wave heading of 45 degrees

Fig. 15: Time series of motions in moderate sea state with 45 degrees wave heading

Fig. 16: Time series of effective tension of mooring lines for moderate sea state

Fig. 17: Effective tension spectra of mooring lines in moderate sea state

Fig. 18: Time series of motions for environmental conditions corresponding to rated wind speed

Fig. 19: Motion response spectra of surge, sway, heave, roll, pitch and yaw motions for environmental conditions corresponding to rated wind speed

Fig. 20: Time series of effective tension of mooring lines in rated wind speed

Fig. 21: Spectra of effective tension for mooring lines for environmental condition that corresponds to rated wind speed

Fig. 22: Time series of turbine functionality for environmental condition that corresponds to rated wind speed

Fig. 23: Spectra of wind turbine functionality data for environmental condition that corresponds to rated wind speed

Fig. 24: Time series of motions for environmental condition that corresponds to over rated wind speed

Fig. 25: Motion response spectra of surge, sway, heave, roll, pitch and yaw motions for environmental condition that corresponds to over rated wind speed

Fig. 26: Time series of effective tension of mooring lines for environmental condition that corresponds to over rated wind speed

Fig. 27: Spectra of effective tension of mooring lines for environmental condition that corresponds to over rated wind speed

Fig. 28: Time series of turbine functionality for environmental condition that corresponds to over rated wind speed

Fig. 29: Spectra of turbine functionality data for environmental condition that corresponds to over rated wind speed

Fig. 30: Time series of turbine electrical torque for environmental condition that corresponds to over rated wind speed

Fig. 31: Spectrum of turbine rotor aerodynamic power for environmental condition that corresponds to over rated wind speed

Table 1: Characteristics of the tower of the wind turbine [32]

Property	Value
Elevation to tower base (platform top) above MSL [m]	10
Elevation to tower top (yaw bearing) above MSL [m]	87.6
Overall (integrated) tower mass [kg]	250,000
Center of Gravity (CoG) location of tower above MSL along tower centerline [m]	43.4
Elevation to tower base (platform top) above MSL [m]	10

Table 2: Characteristics of the wind turbine [31,32]

Property	Value
Nacelle mass [kg]	240,000
Rotor mass [kg]	110,000
Wind turbine (WT) CoG [m]	(-0.2, 0.0, 70)
Total mass of WT [kg]	600,000
Total WT mass moment of inertia about X axis (I_{XX}) [kg*m^2]	3.77exp.+9
Total WT mass moment of inertia about Y axis (I_{YY}) [kg*m^2]	3.66exp.+9
Total WT mass moment of inertia about Z axis (I_{ZZ}) [kg*m^2]	1.12exp.+8

Table 3: Characteristics of different designs of V-shaped semisubmersible, V55, V60, V65 and V75, considering the modification of the angle between pontoons, θ.

Characteristics	Alternative designs of V-shaped semisubmersible			
	V55	V60	V65	V75
Floater steel mass [kg]	1,280,000	1,282,000	1,283,000	1,285,000
Water ballast mass[kg]	4,335,000	4,338,000	4,346,000	4,354,000
Total mass [kg]	6,374,000	6,379,000	6,388,000	6,399,000
Submerged volume [m^3]	6,218	6,225	6,231	6,241
X_{CoG} [m]	-31.2	-30.6	-29.8	-27.9
X_{CoB} [m]	-31.3	-30.6	-29.8	-27.9
Z_{CoG} [m]	-13.1	-13.0	-13.0	-13.1
Z_{CoB} [m]	-19.8	-19.8	-19.8	-19.8
GM_L [m]	4.9	4.3	3.7	2.5
GM_T [m]	2.7	4.3	6.0	9.6

Table 4: Characteristics of alternative designs of V-shaped semisubmersible considering increased pontoon and columns dimensions

Characteristics	Alternative designs of V-shaped semisubmersible		
	$V60_{al1}$	$V60_{al2}$	$V60_{al3}$
Distance between columns [m]	50	70	60
Pontoon dimensions; widthxheight [mxm]	9x5	7x4	9x5
Diameter of columns [m]	9	7	9
Floater steel mass [kg]	1,498,000	1,385,000	1,630,000
Water ballast [kg]	7,082,000	4,810,000	7,873,000
Total mass [kg]	9,340,000	6,954,000	10,263,000
Submerged volume [m^3]	9,113	6,785	10,013
X_{CoG} [m]	-25.8	-35.2	-30.6
X_{CoB} [m]	-25.8	-35.2	-30.6
Z_{CoG} [m]	-14.9	-14.2	-16.0
Z_{CoB} [m]	-18.8	-20.33	-19.4
GM_L [m]	4.9	7.7	8.1
GM_T [m]	4.9	7.7	8.1

Table 5: CoB, CoG and mass moment of inertia of the $V60_{al3}$

Property	Value
CoB (x, y, z) [m]	(-30.6, 0.0, -19.4)
CoG (x, y, z) [m]	(-30.6, 0.0, -16.0) m
I_{xx} [kg*m^2]	1.29exp.+10
I_{yy} [kg*m^2]	2.18exp.+10
I_{zz} [kg*m^2]	1.79exp.+10
I_{yx} [kg*m^2]	3.20exp.+6
I_{zx} [kg*m^2]	-6.4exp.+9
I_{zy} [kg*m^2]	9.87exp.+5

Table 6: Mooring line characteristics

Variables	Value
Length of each line [m]	453
Mass per meter [kg/m]	117
Equivalent Axial stiffness [N]	3.0exp.+9
Diameter [m]	0.138
Drag coefficient	1.2
Clump mass [m]	37,000
Clump mass volume [m^3]	4.4

Table 7: Coordinates of fairlead and anchoring points of the mooring lines ML1, ML2 and ML3

Variables	Value
Fairlead of ML1 (x, y, z) [m]	(4.5, 0, -18)
Fairlead of ML2 (x, y, z) [m]	(-55.8, 32.3, -18)
Fairlead of ML3 (x, y, z) [m]	(-55.8, -32.3, -18)
Anchor point of ML1 (x, y, z) [m]	(450, 0, -100)
Anchor point of ML2 (x, y, z) [m]	(-441.7, 255, -100)
Anchor point of ML3 (x, y, z) [m]	(-441.7, -255, -100)

Table 8: Added mass coefficients calculated in WAMIT (at infinite frequency)

Variables	Value
Surge [kg]	4.939exp.+6
Sway [kg]	6.772exp.+6
Heave [kg]	1.062exp.+7
Roll [kg*m^2]	5.488exp.+9
Pitch [kg*m^2]	1.022exp.+10
Yaw [kg*m^2]	1.472exp.+10

Table 9: Hydrostatic restoring coefficients calculated in WAMIT

Variables	Value
Heave [N/m]	1.91exp.+6
Roll [Nm]	7.86exp.+8
Pitch [Nm]	3.07exp.+9

Table 10: Statistical characteristics of motion and tension responses for wave only extreme environmental conditions

Item	Characteristics	Wave heading 0 degrees	Wave heading45 degrees
Tension (kN)	Mean	1,200	1,230
	STD	190	147
	Min	541	644
	Max	2,720	2,250
Surge (m)	Mean	-6.39	-6.76
	STD	2.39	1.74
	Min	-13.50	-11.91
	Max	2.76	-0.30
Sway (m)	Mean	0.0	4.26
	STD	0.0	2.11
	Min	0.0	-1.49
	Max	0.0	13.38
Heave (m)	Mean	-0.07	0.01
	STD	1.56	1.29
	Min	-6.63	-5.12
	Max	4.38	4.06
Roll (deg)	Mean	0.0	-0.07
	STD	0.0	0.82
	Min	-0.03	-3.33
	Max	0.03	2.35
Pitch (deg)	Mean	-0.10	-0.23
	STD	1.97	1.58
	Min	-6.71	-4.97
	Max	7.28	5.70
Yaw (deg)	Mean	0.0	-2.9
	STD	0.0	1.8
	Min	0.0	-10.0
	Max	0.0	2.8

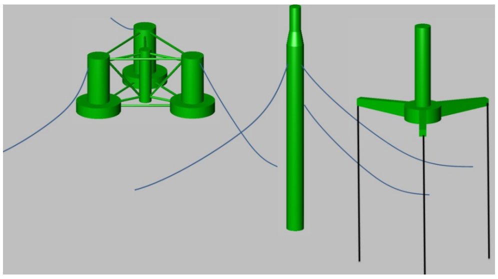

Figure 1: Different floating concepts: semisubmersible, spar buoy and tension leg platform

Figure 2: Braceless semisubmersible offshore wind turbine (Fukushima FORWARD [12])

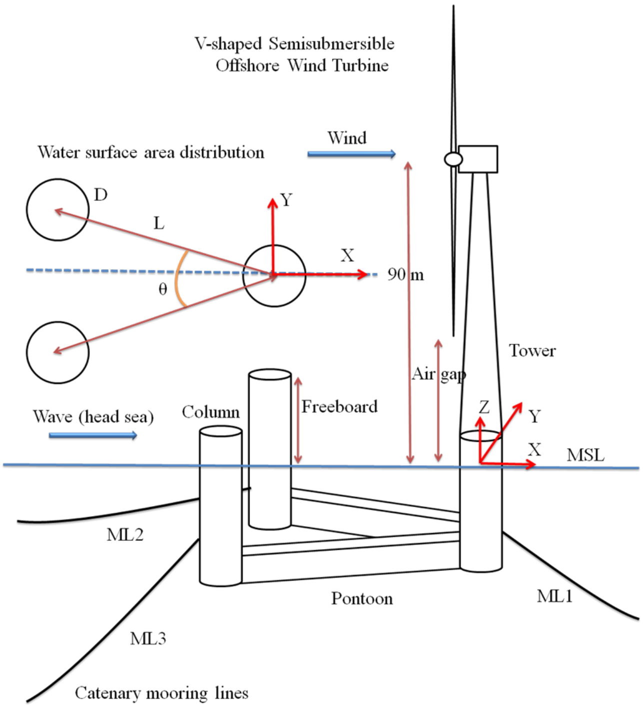

Figure 3: Schematic layout of the V-shaped semisubmersible offshore wind turbine

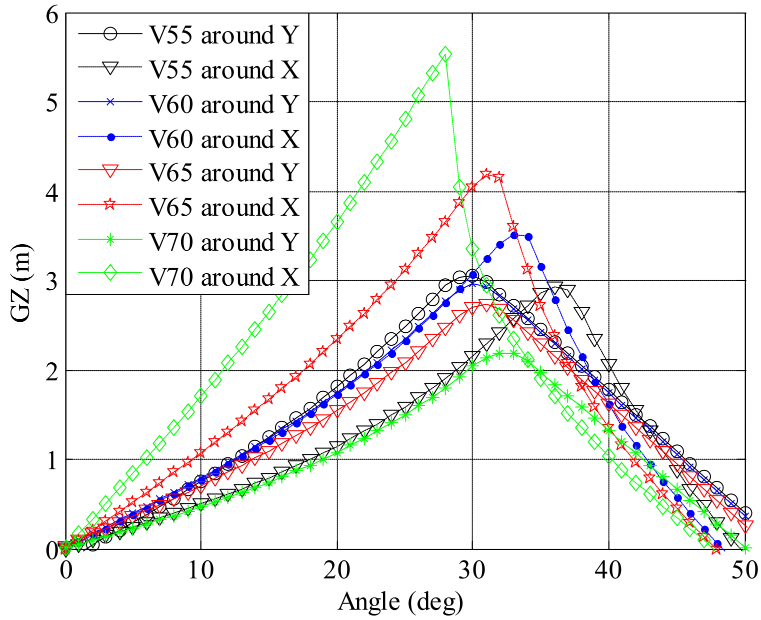

Figure 4: Transversal (around X-axis) and longitudinal (around Y-axis) GZ (righting arms) curves of V55, V60, V65 and V75 V-shaped semisubmersible offshore wind turbine

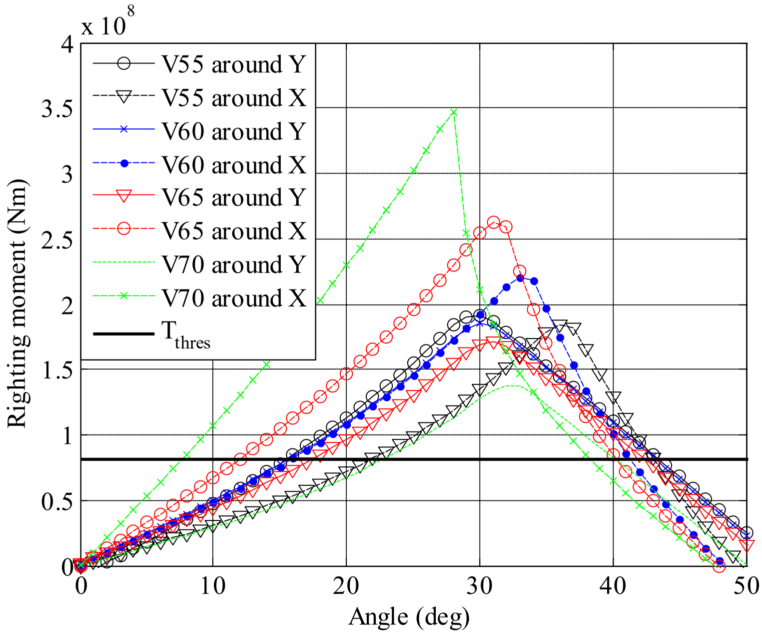

Figure 5: Transversal (around X-axis) and longitudinal (around Y-axis) righting moment curves of the V55, V60, V65 and V75 V-shaped semisubmersible offshore wind turbine

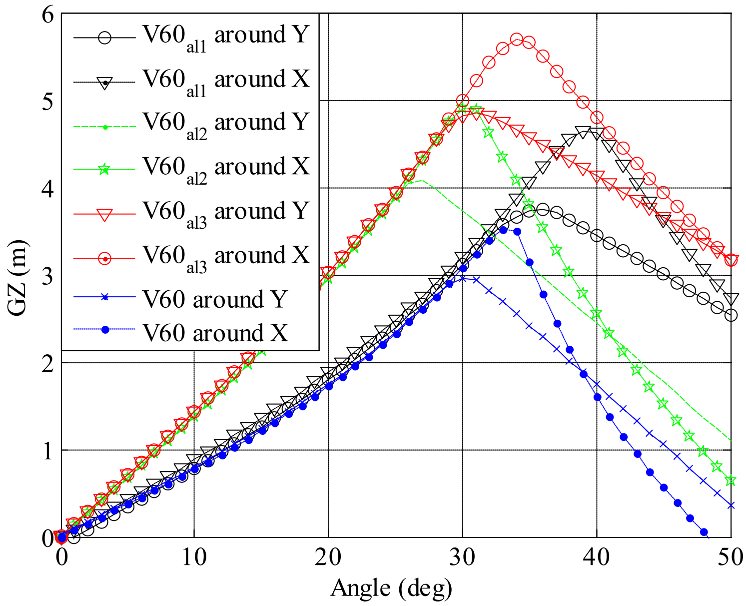

Figure 6: Transversal (around X-axis) and longitudinal (around Y-axis) GZ (righting arms) curves of $V60_{al1}$, $V60_{al2}$, $V60_{al3}$, and V60 V-shaped semisubmersible offshore wind turbine

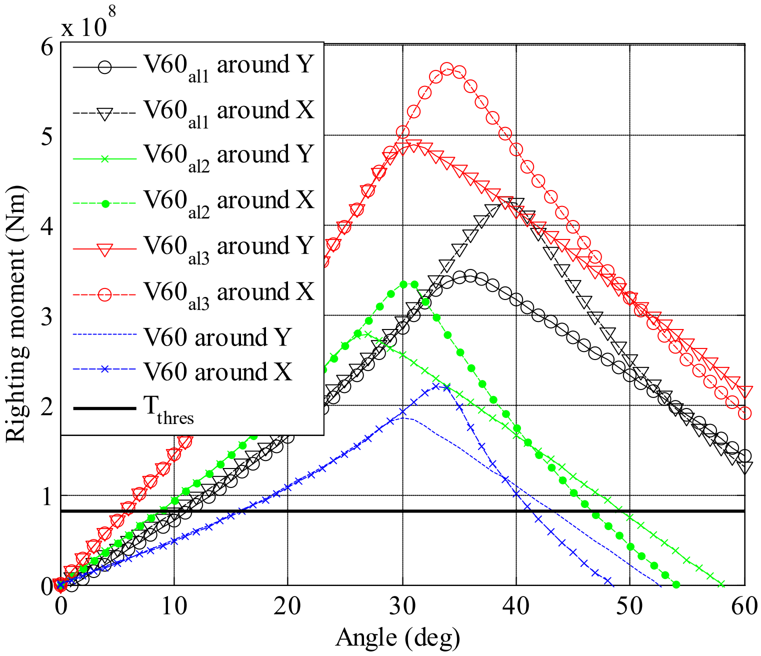

Figure 7: Transversal (around X-axis) and longitudinal (around Y-axis) righting moment curves of the $V60_{al1}$, $V60_{al2}$, $V60_{al3}$, and V60 V-shaped semisubmersible offshore wind turbine

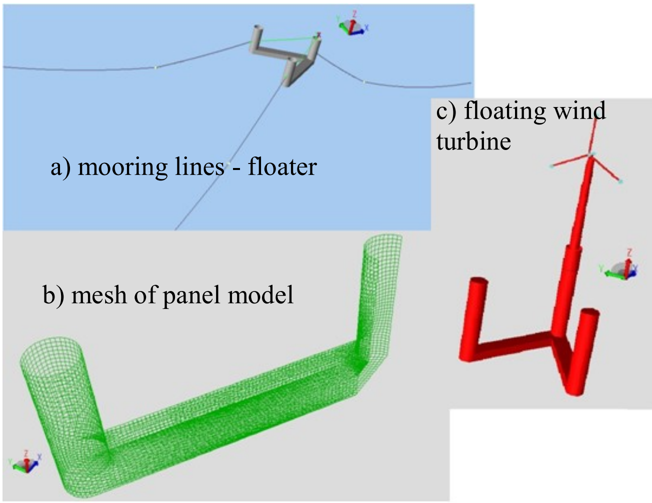

Figure 8: Modeling of the V-shaped semisubmersible: a) mooring lines and platform in SIMA, b) panel mesh for half-geometry in WAMIT (15,640 elements for entire platform) and c) V-shaped floating wind turbine in Genie

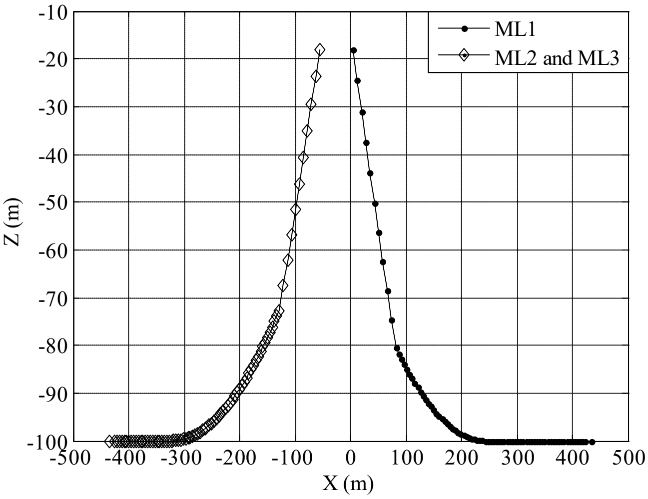

Figure 9: Static equilibrium configuration of catenary mooring lines

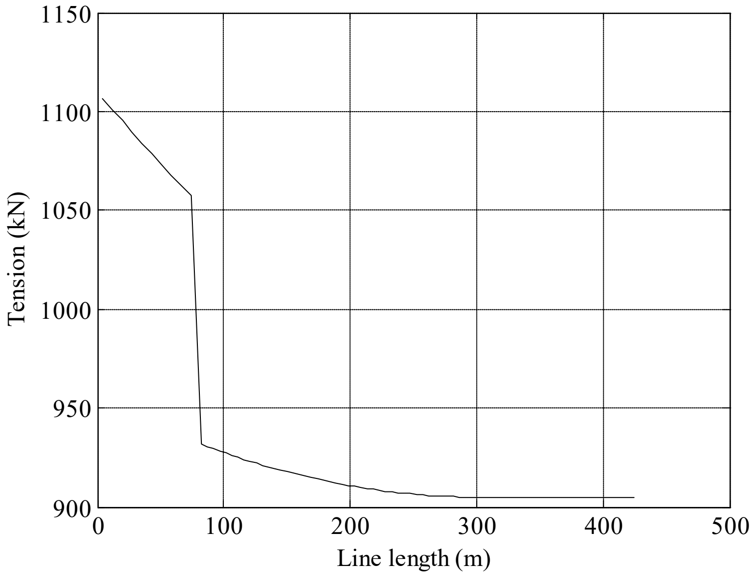

Figure 10: Axial effective tension in mooring lines in static equilibrium configuration, the clump mass effect is clear at X=82 m to increase the tension at upper part of the line from 930 kN to 1057 kN

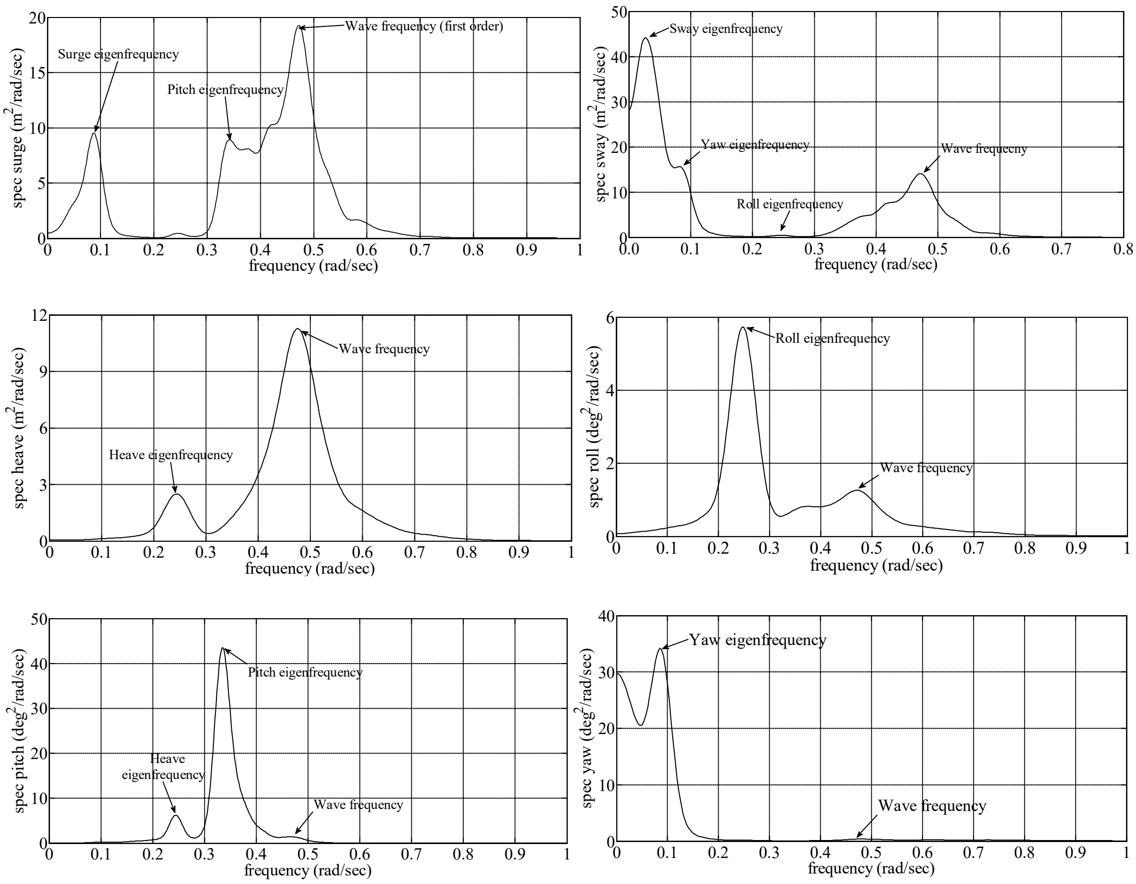

Figure 11: Motion response spectra of surge, sway, heave, roll, pitch and yaw motions for wave heading of 45 degrees.

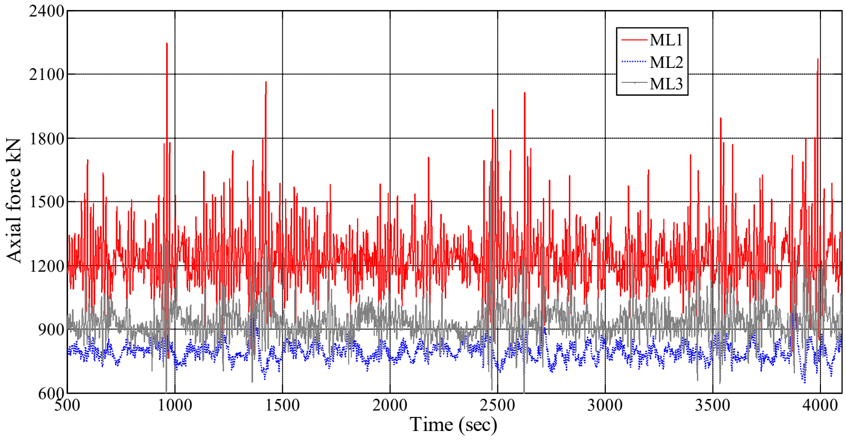

Figure 12: Time series of tension of mooring lines in extreme conditions for wave heading of 45 degrees

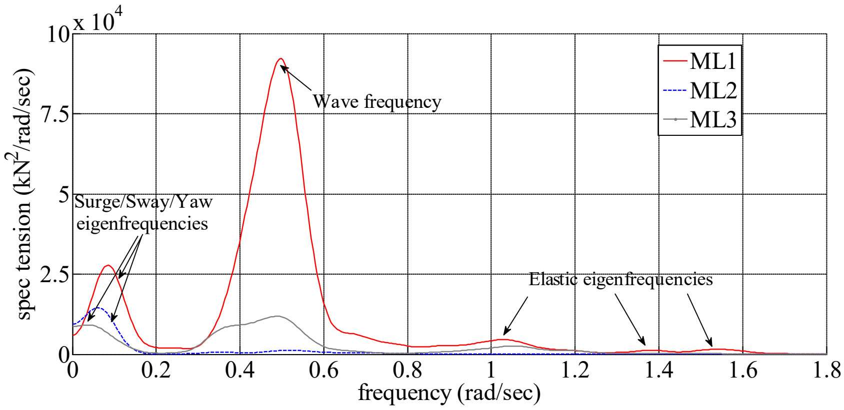

Figure 13: Spectra of tension of mooring lines in extreme sea state for wave heading of 45 degrees

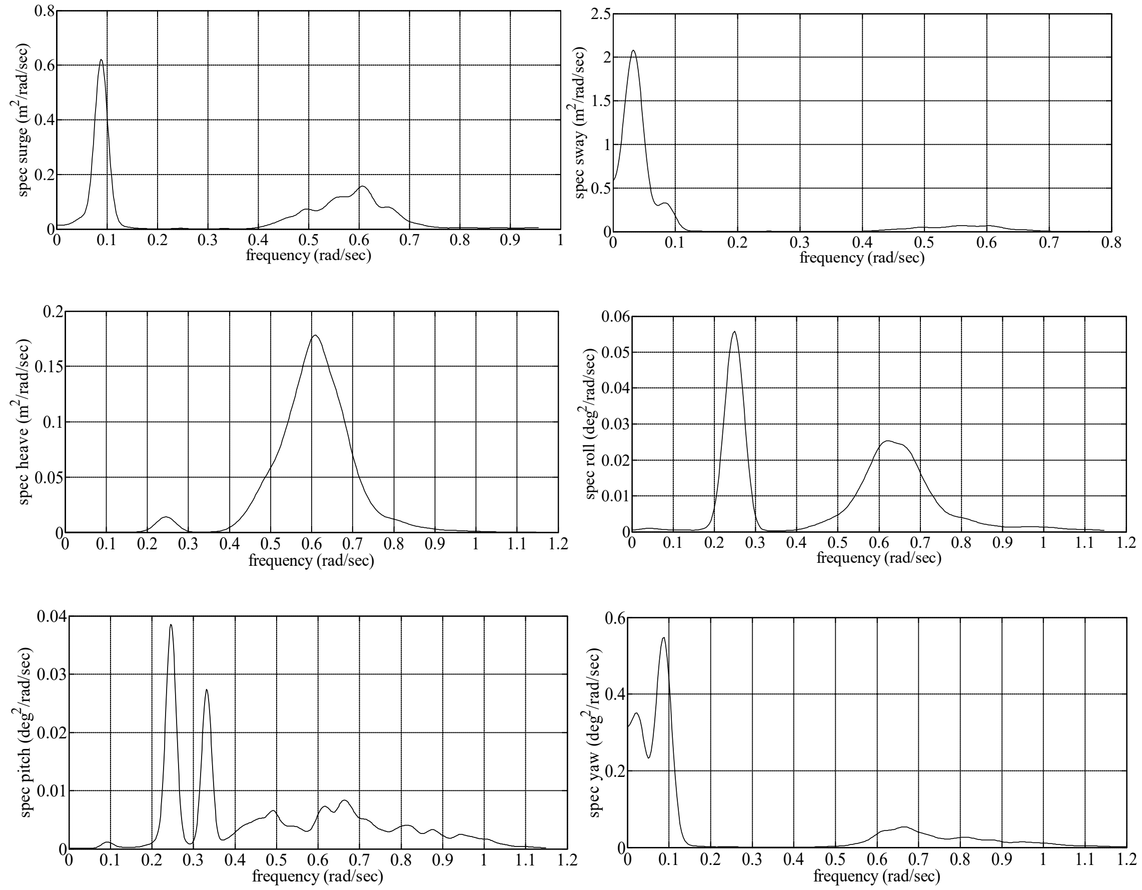

Figure 14: Motion response spectra of surge, sway, heave, roll, pitch and yaw motions for a moderate sea state with wave heading of 45 degrees

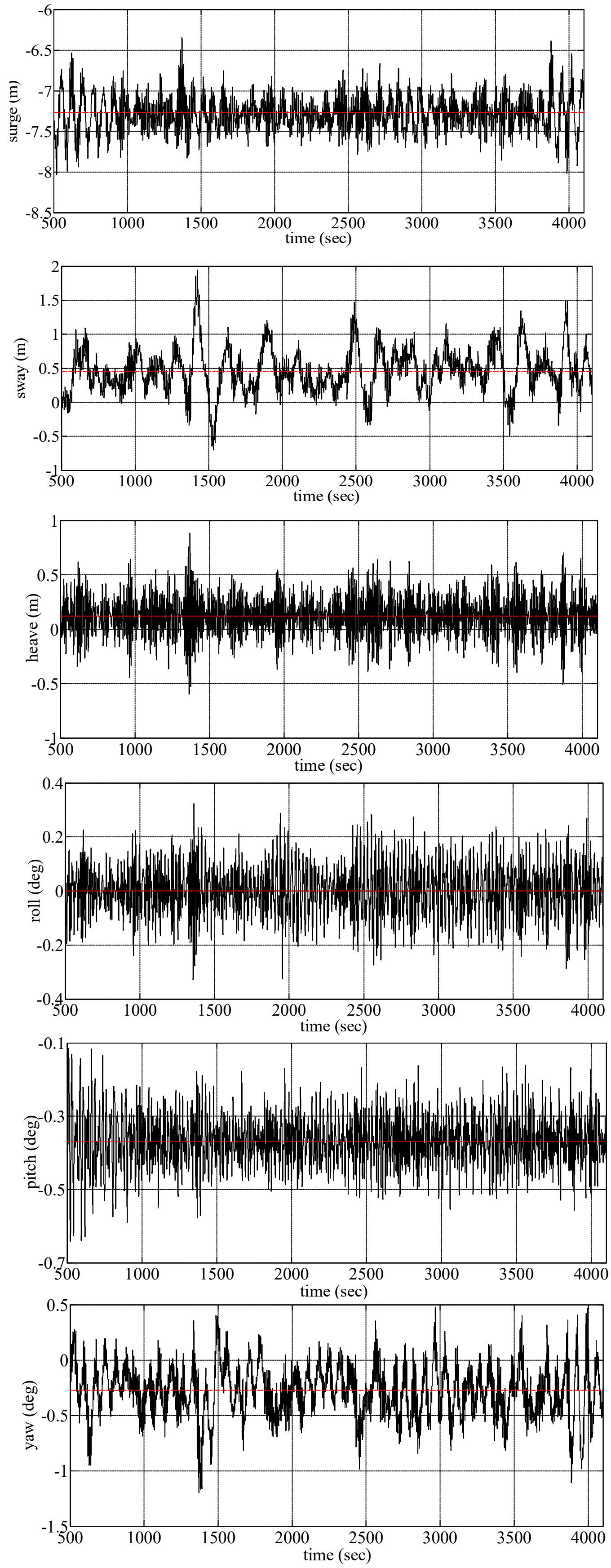

Fig. 15: Time series of motions in moderate sea state with 45 degrees wave heading

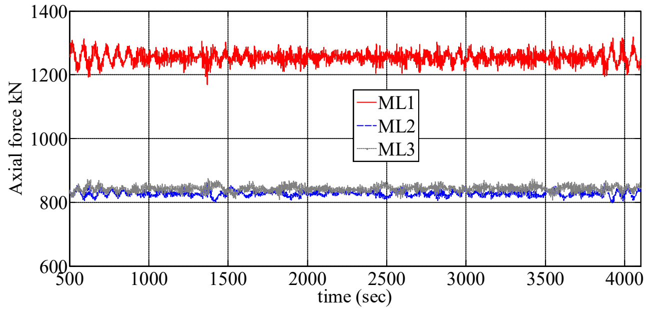

Fig. 16: Time series of effective tension of mooring lines for moderate sea state

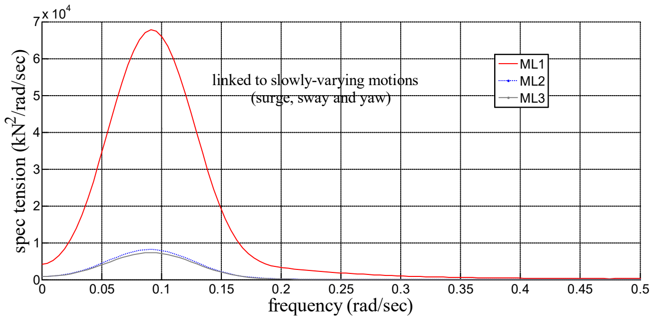

Fig. 17: Effective tension spectra of mooring lines in moderate sea state

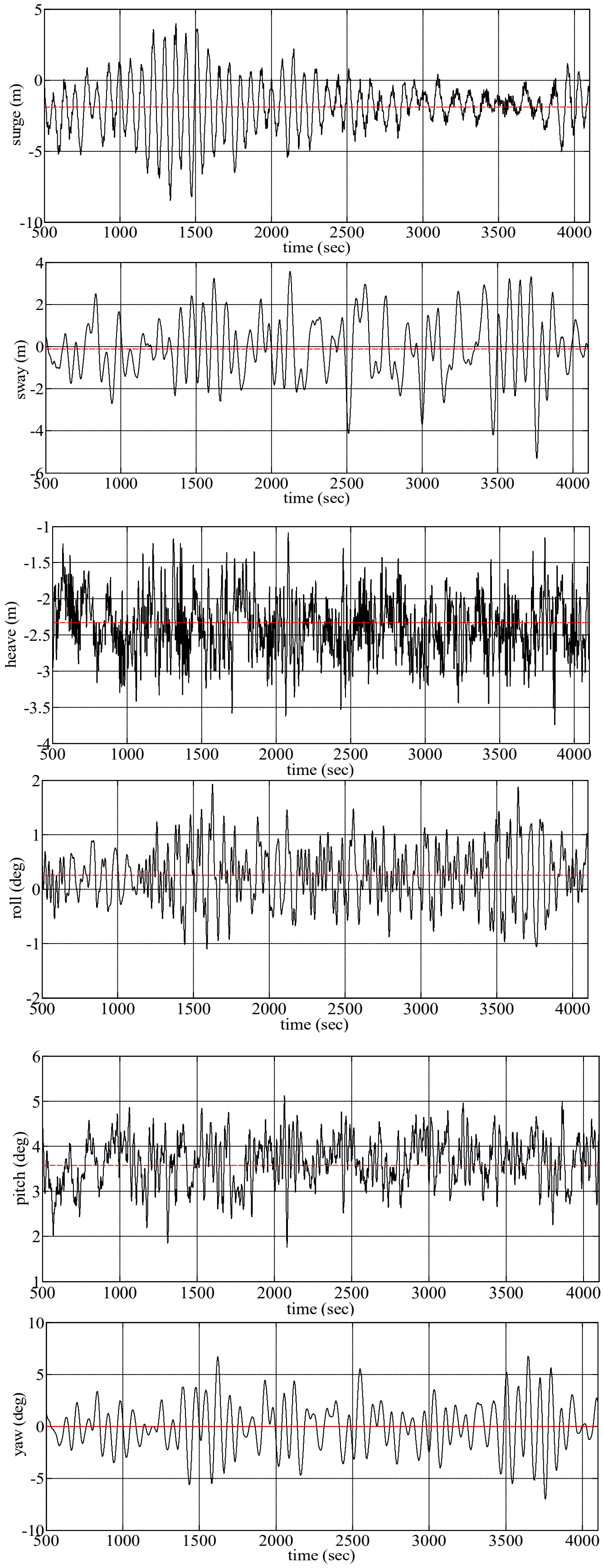

Fig. 18: Time series of motions for environmental conditions corresponding to rated wind speed

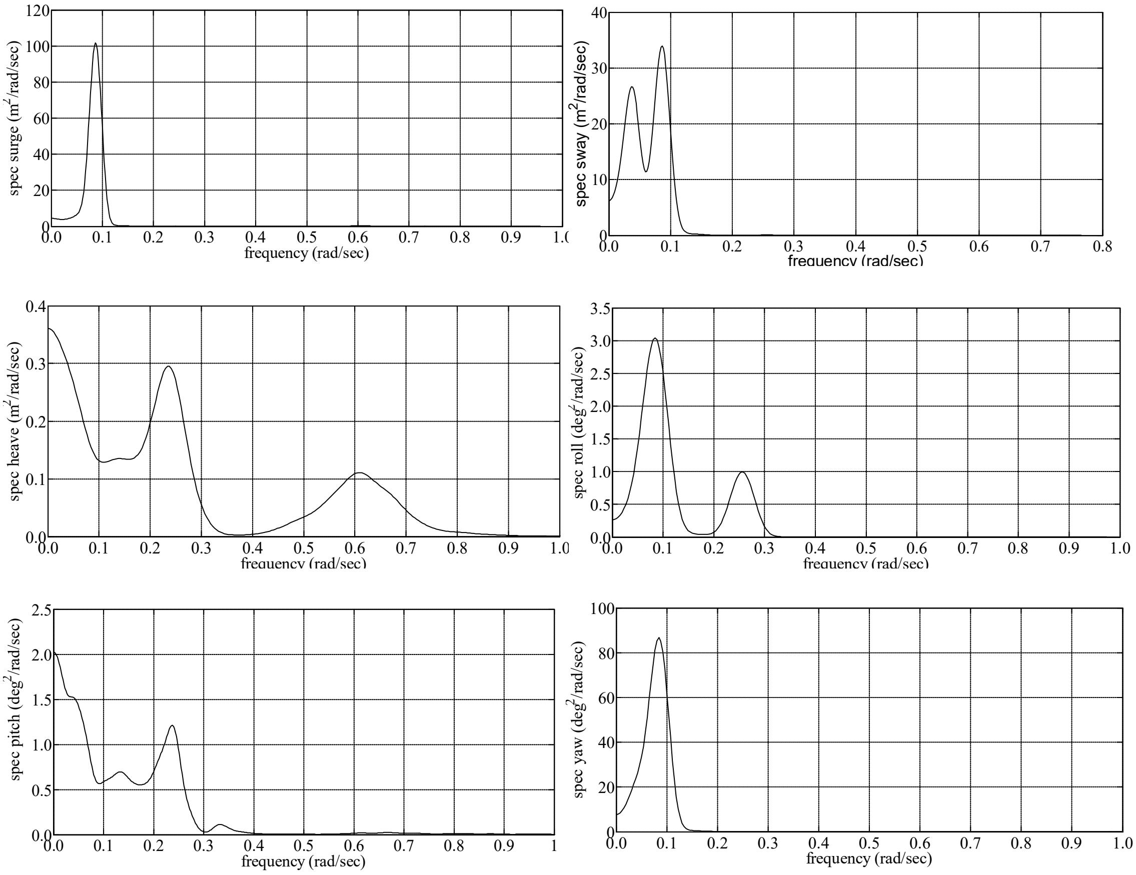

Fig. 19: Motion response spectra of surge, sway, heave, roll, pitch and yaw motions for environmental conditions corresponding to rated wind speed

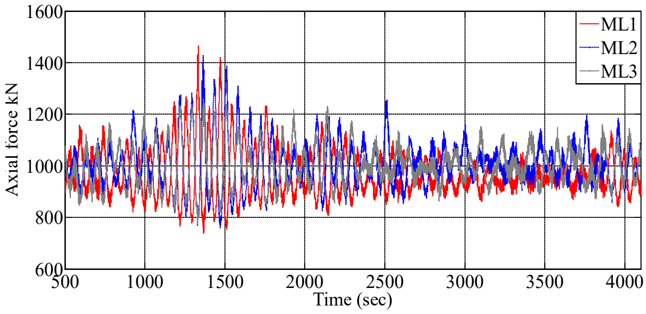

Fig. 20: Time series of effective tension of mooring lines in rated wind speed

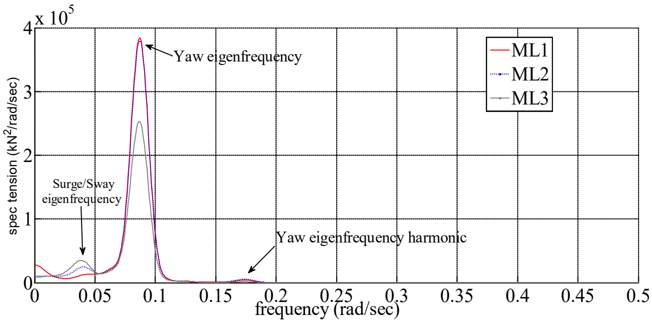

Fig. 21: Spectra of effective tension for mooring lines for environmental condition that corresponds to rated wind speed

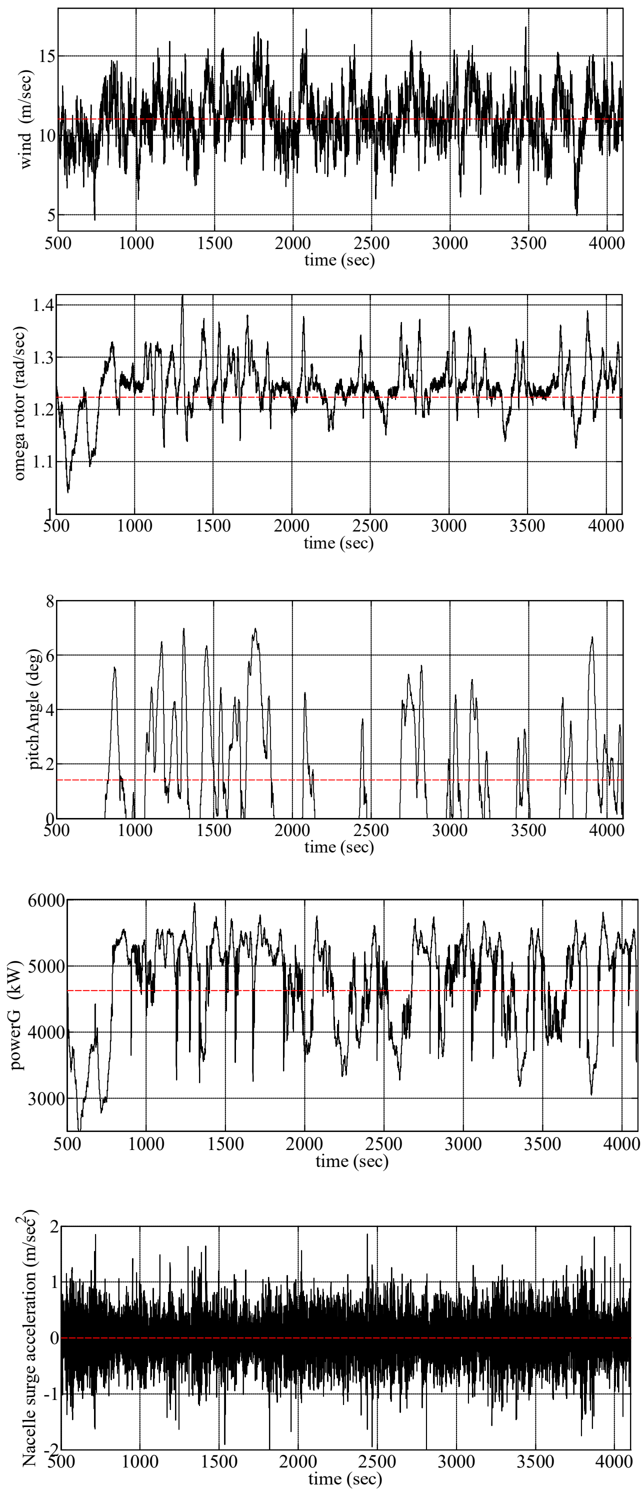

Fig. 22: Time series of turbine functionality for environmental condition that corresponds to rated wind speed

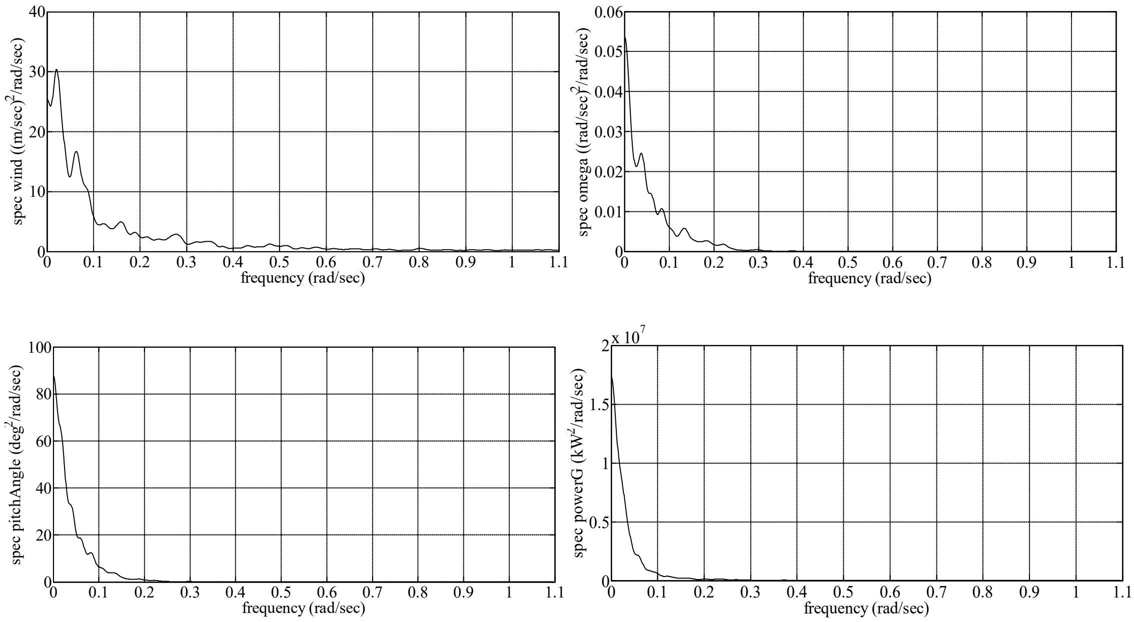

Fig. 23: Spectra of wind turbine functionality data for environmental condition that corresponds to rated wind speed

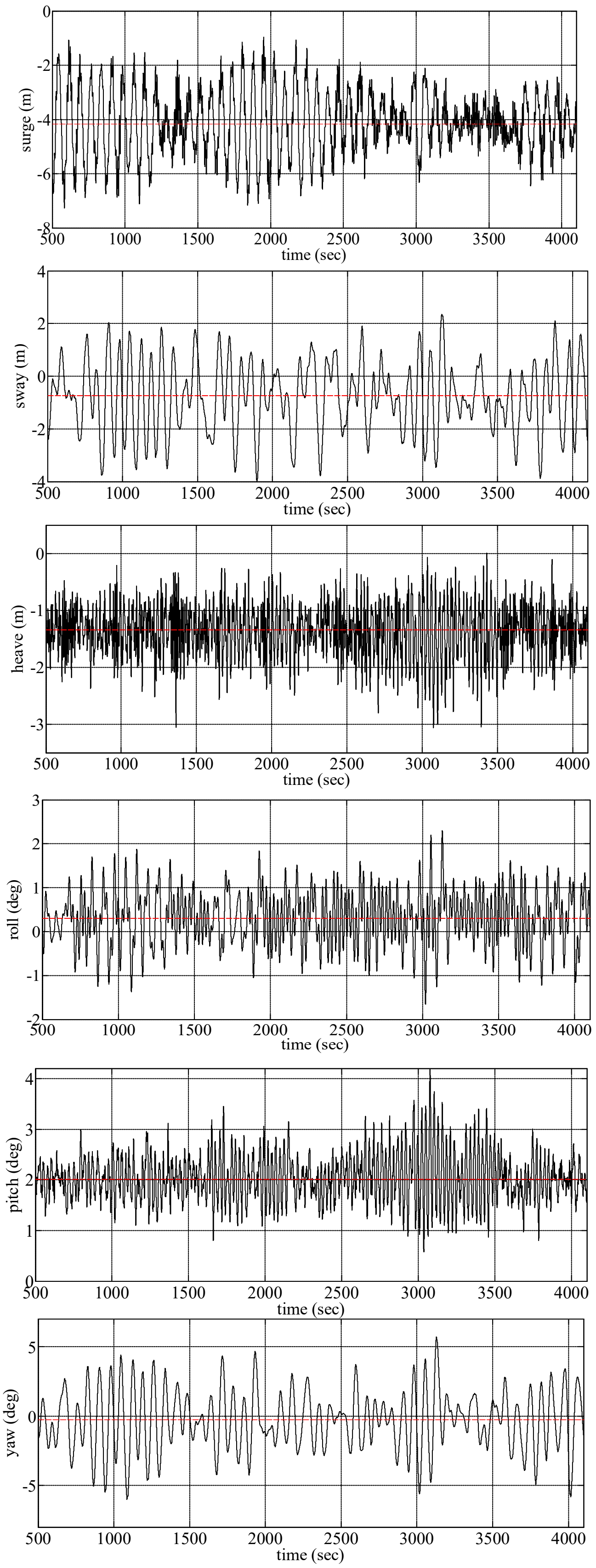

Fig. 24: Time series of motions for environmental condition that corresponds to over rated wind speed

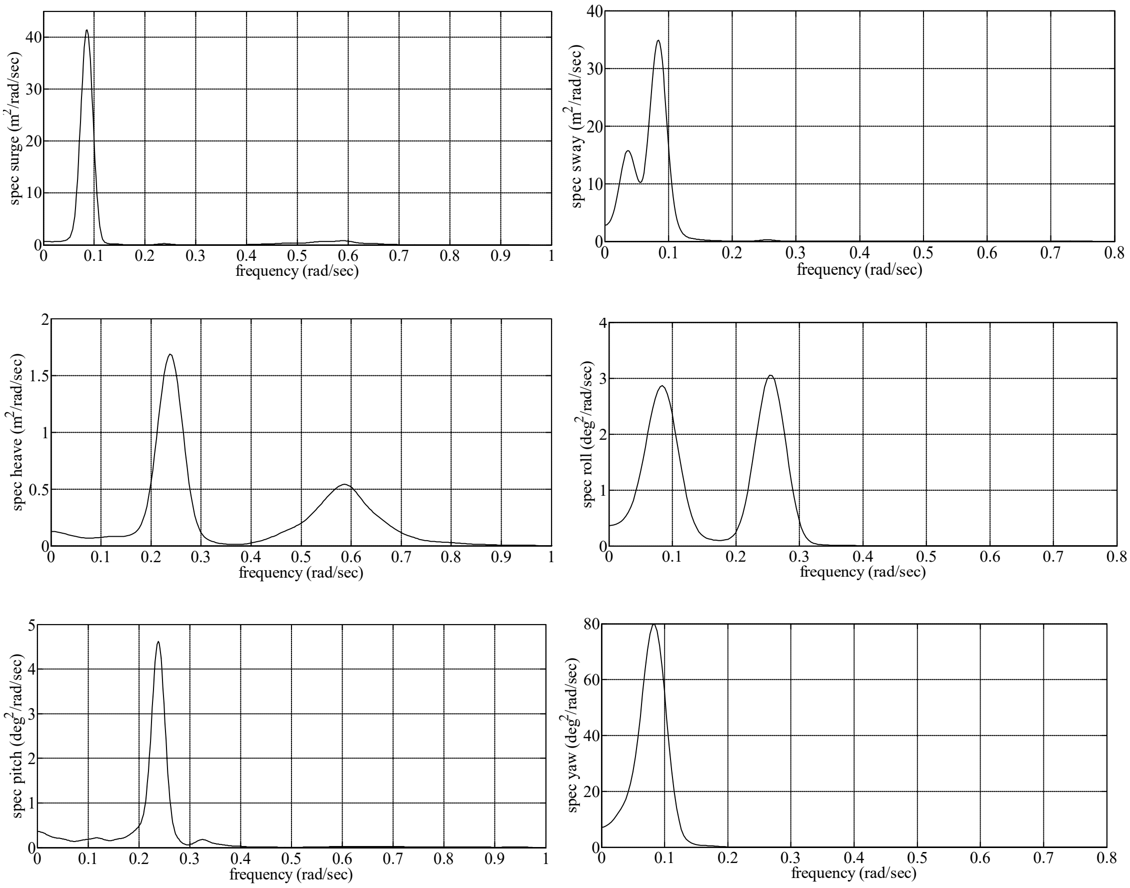

Fig. 25: Motion response spectra of surge, sway, heave, roll, pitch and yaw motions for environmental condition that corresponds to over rated wind speed

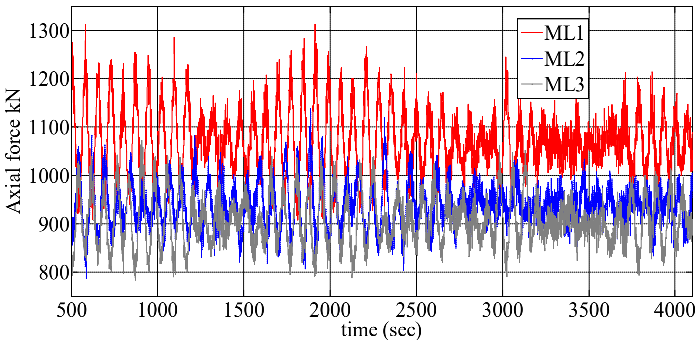

Fig. 26: Time series of effective tension of mooring lines for environmental condition that corresponds to over rated wind speed

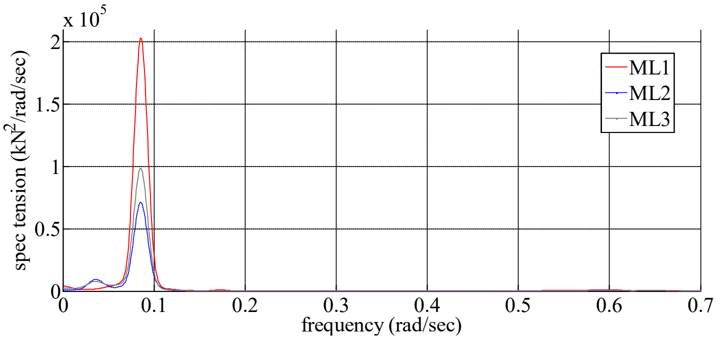

Fig. 27: Spectra of effective tension of mooring lines for environmental condition that corresponds to over rated wind speed

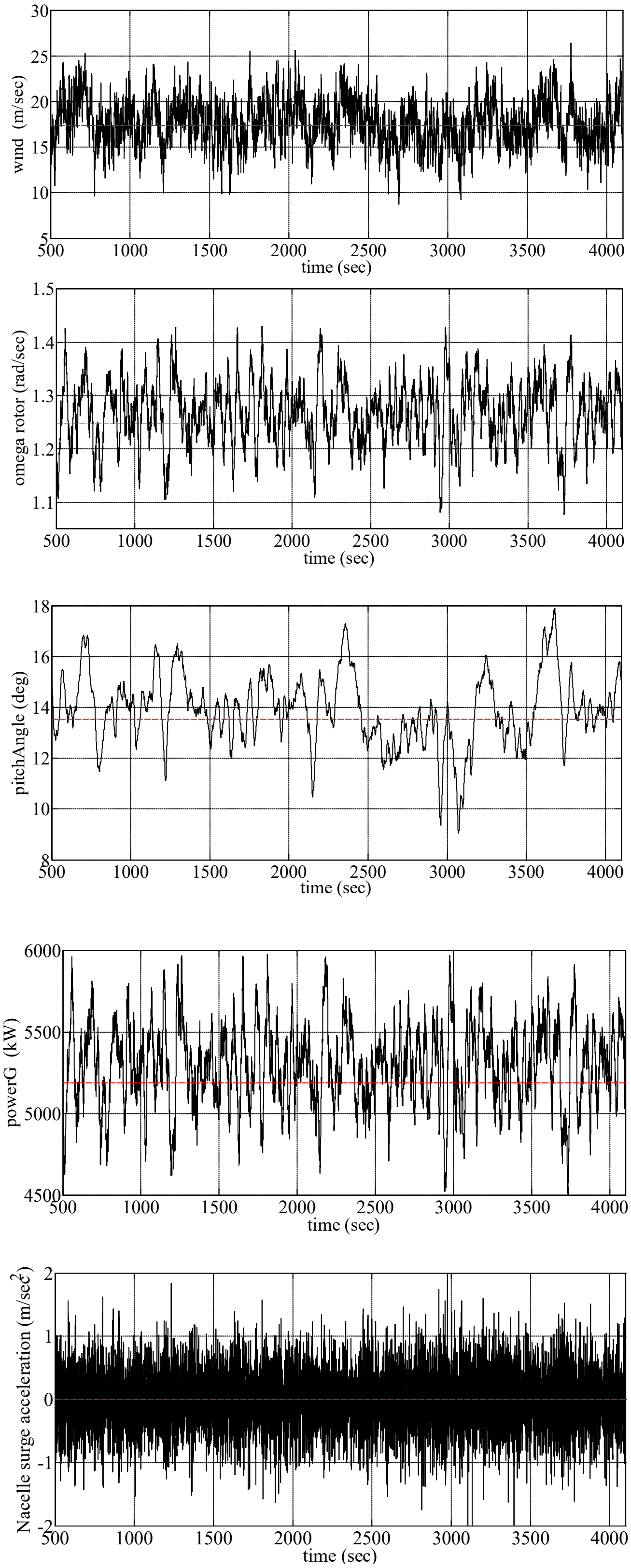

Fig. 28: Time series of turbine functionality for environmental condition that corresponds to over rated wind speed

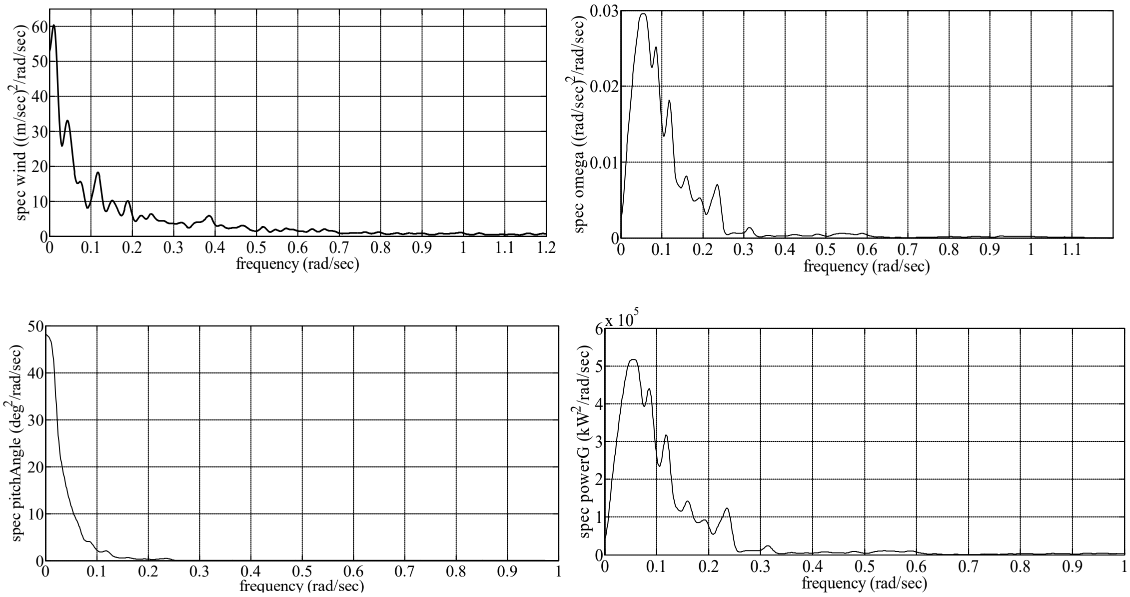

Fig. 29: Spectra of turbine functionality data for environmental condition that corresponds to over rated wind speed

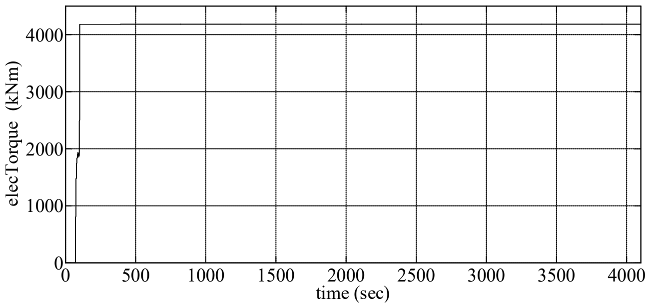

Fig. 30: Time series of turbine electrical torque for environmental condition that corresponds to over rated wind speed

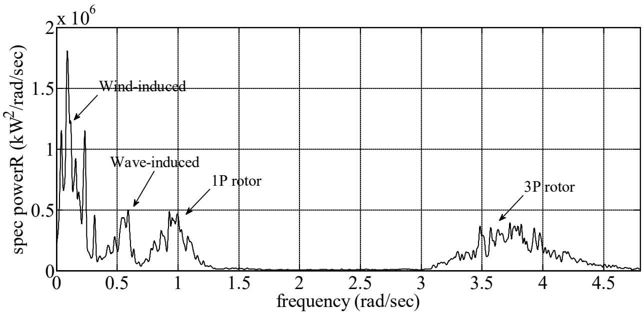

Fig. 31: Spectrum of turbine rotor aerodynamic power for environmental condition that corresponds to over rated wind speed